

# Thermodynamic properties of highly frustrated quantum spin ladders: influence of many-particle bound states

A. Honecker,<sup>1,2</sup> S. Wessel,<sup>3</sup> R. Kerkdyk,<sup>2</sup> T. Pruschke,<sup>2</sup> F. Mila,<sup>4</sup> and B. Normand<sup>5</sup>

<sup>1</sup>*Laboratoire de Physique Théorique et Modélisation, CNRS UMR 8089, Université de Cergy-Pontoise, F-95302 Cergy-Pontoise Cedex, France*

<sup>2</sup>*Institut für Theoretische Physik, Georg-August-Universität Göttingen, 37077 Göttingen, Germany*

<sup>3</sup>*Institut für Theoretische Festkörperphysik, JARA-FIT and JARA-HPC, RWTH Aachen University, 52056 Aachen, Germany*

<sup>4</sup>*Institute of Theoretical Physics, Ecole Polytechnique Fédérale Lausanne, CH-1015 Lausanne, Switzerland*

<sup>5</sup>*Department of Physics, Renmin University of China, Beijing 100872, P. R. China*

(Dated: November 4, 2015)

Quantum antiferromagnets have proven to be some of the cleanest realizations available for theoretical, numerical, and experimental studies of quantum fluctuation effects. At finite temperatures, however, the additional effects of thermal fluctuations in the restricted phase space of a low-dimensional system have received much less attention, particularly the situation in frustrated quantum magnets, where the excitations may be complex collective (bound or even fractionalized) modes. We investigate this problem by studying the thermodynamic properties of the frustrated two-leg  $S = 1/2$  spin ladder, with particular emphasis on the fully frustrated case. We present numerical results for the magnetic specific heat and susceptibility, obtained from exact diagonalization and quantum Monte Carlo studies, which we show can be rendered free of the sign problem even in a strongly frustrated system and which allow us to reach unprecedented sizes of  $L = 200$  ladder rungs. We find that frustration effects cause an unconventional evolution of the thermodynamic response across the full parameter regime of the model. However, close to the first-order transition they cause a highly anomalous reduction in temperature scales with no concomitant changes in the gap; the specific heat shows a very narrow peak at very low energies and the susceptibility rises abruptly at extremely low temperatures. Unusually, the two quantities have different gaps over an extended region of the parameter space. We demonstrate that these results reflect the presence of large numbers of multi-particle bound-state excitations, whose energies fall below the one-triplon gap in the transition region.

PACS numbers: 75.10.Jm, 75.40.Gb, 75.40.Mg

## I. INTRODUCTION

Quantum magnets rank among the simplest model systems in condensed matter physics, but nonetheless exhibit some of its most fundamental phenomena, including quantum phase transitions, symmetry-breaking and restoration, collective and fractionalized excitations, topological order, and complex entanglement of the quantum wave function. From a theoretical point of view, these phenomena arise even in models with only the most elementary magnetic interaction, described by the Heisenberg model [1], and depend crucially on the geometry of the lattice. In low-dimensional systems, quantum fluctuation effects are strong, and models in one spatial dimension provide particularly good examples of exotic phenomena [2], not least the gapped “Haldane” state of the nearest-neighbor spin-1 chain [3] and the exactly dimerized ground state, with fractional “spinon” excitations, of the frustrated spin-1/2  $J_1$ - $J_2$  chain [4, 5]. In higher dimensions, models on bipartite lattices tend to show semi-classical long-ranged magnetic order, whereas geometrically frustrated lattices offer both analogs of the unconventional ground states of quantum spin chains and uniquely high-dimensional phases such as the quantum spin liquid. [6–9].

A frustrated two-dimensional system related to the  $J_1$ -

$J_2$  chain is the Shastry-Sutherland model [10], which exhibits an exact dimer-singlet ground state. The compound  $\text{SrCu}_2(\text{BO}_3)_2$ , based on  $S = 1/2$   $\text{Cu}^{2+}$  ions, provides not only a good realization of this model, but one that is believed to be located close to a frustration-induced quantum phase transition out of the dimer-singlet phase [11–14]. As a consequence,  $\text{SrCu}_2(\text{BO}_3)_2$  displays a number of exotic properties, including a magnetization curve that exhibits many plateaus [12, 15–18]. The origin of this unusual behavior lies in the strong suppression of kinetic energy contributions from the triplet excitations, due to the almost perfectly frustrated coupling of the dimers in the Shastry-Sutherland model [19]. When magnetic excitations become highly localized in this way, the related phenomenon of bound-state formation appears. In two-leg spin-1/2 ladders with little or no frustration, bound states are present in the spectrum at higher energies [20, 21], whereas in strongly frustrated systems they can occur at low energies, particularly close to a quantum phase transition as in the Shastry-Sutherland model [19, 22].

The presence of additional low-energy states in the spectrum of a system is expected to have a clear signature in its physical properties. Despite the fact that the thermodynamic properties are frequently used as one of the first experimental characterizations of any new mate-

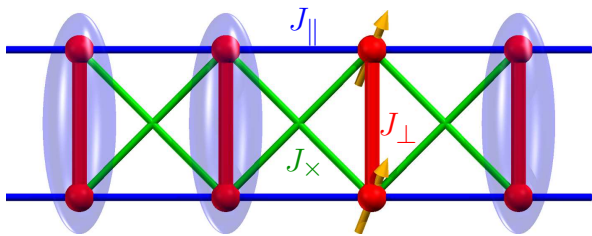


FIG. 1. (Color online) Representation of superexchange interactions in a frustrated spin ladder. Each ladder site (spheres) hosts an  $S = 1/2$  quantum spin and the Heisenberg couplings between spins are specified by the parameters  $J_{\perp}$  for the ladder rungs,  $J_{\parallel}$  for the ladder legs, and  $J_{\times}$  for the cross-plaquette couplings, which we take to be symmetrical. Ellipsoids represent singlet states of the two rung spins and their absence a rung triplet.

rial, their computation actually constitutes a major challenge for theory. Exact results for the finite-temperature properties of truly quantum models are scarce, being restricted to integrable systems such as the nearest-neighbor spin-1/2 Heisenberg chain [23–28], which can be solved by generalizations of the Bethe Ansatz [29, 30].

Among the numerical approaches to this problem, one of the first to be used was the full exact diagonalization (ED) of the Hamiltonian in the exponentially large Hilbert space [31]. Although this method can be extended as far as 24 spin-1/2 sites with current technology [32], standard applications are limited to approximately 20  $S = 1/2$  sites [11], a size with restricted applicability in two and higher dimensions. Another classic approach is the use of high-temperature series expansions [33–35], but frustrated systems such as the Shastry-Sutherland model [36] illustrate the difficulties suffered by this method in accessing the low-temperature regime. Finite-temperature variants of the density-matrix renormalization group (DMRG) technique [37] have been developed into powerful tools for calculating the thermodynamic properties of one-dimensional systems [38–40], but despite the development of modern matrix-product-state DMRG formulations [41], these transfer-matrix RG (TMRG) methods have mostly remained limited to one dimension. Quantum Monte Carlo (QMC) simulations provide the most flexible approach in higher dimensions, and are able to resolve the primary features of the thermodynamic quantities for models that are at most weakly frustrated [42–44], but these break down in more strongly frustrated systems due to the notorious QMC sign problem.

As a consequence of these technical limitations, there has been little systematic investigation of the finite-temperature response of quantum spin systems with strong geometrical frustration, and thus the influence both of bound states in the excitation spectrum and of proximity to a quantum critical point on the thermodynamic properties remains poorly understood. Here we provide a detailed analysis of these issues using the model

of the fully frustrated two-leg spin-1/2 ladder, which is shown in Fig. 1. A significant amount of information is already available concerning the zero-temperature properties of this precise model [45–51] and variants thereof [52–59]. Like the Shastry-Sutherland model, it exhibits a phase with a dimer-singlet ground state, fully localized triplet excitations, and a first-order phase transition [45, 47]. The importance of multi-triplet bound-state excitations was also recognized in early analytical studies of the fully frustrated ladder [45, 47] and observed in a DMRG calculation [49].

Building on these analytical properties, we perform and interpret detailed numerical calculations of the magnetic specific heat and susceptibility of the fully frustrated ladder. With a view to a complete microscopic understanding of the spectrum, and profiting from the very short correlation length of the fully frustrated system, our tool of choice for this investigation is ED rather than TMRG or DMRG. We will show that this model permits a detailed analysis of the excitation spectrum, which shows a highly unconventional emergence of multi-particle bound states involving very many rungs near the quantum phase transition. Because this feature exceeds the system-size limitations of ED, we exploit the properties of the model to express the spin Hamiltonian in the dimer basis and achieve the ability to perform QMC simulations completely free of the sign problem. These we employ to compute the numerically exact specific heat and susceptibility for ladders of up to 400 spins, which we show is well in the thermodynamic limit even for systems arbitrarily close to the quantum phase transition.

The structure of this article is as follows. In Sec. II we introduce the fully frustrated ladder model and highlight some of its analytical properties. These allow us to review the ground-state phase diagram, to discuss the nature of the low-energy excitations in the two different phases, which include exact and perfectly localized bound states, and to highlight the appearance of many low-lying states near the phase transition. We then use these properties in an analytical discussion of a simple approximation to the thermodynamics of the fully frustrated ladder in the rung-singlet phase and compare its qualitative features with those of unfrustrated ladders. Because a systematic analysis of thermodynamic properties, particularly near the phase transition, requires exact numerical results, in Sec. III we explain how the specific properties of the fully frustrated ladder may be exploited to perform maximally efficient ED calculations and, despite the frustration, sign-problem-free QMC simulations. Section IV presents and compares the results we obtain from these numerical calculations for the magnetic specific heat and susceptibility over the full range of temperatures, for a selection of fully frustrated ladders with different coupling ratios. In Sec. V we provide some analytical interpretations of our results, by comparing them with small- and large-cluster approximations, and by discussing the different energy scales characterizing the dramatic effects occurring near the phase transition. Our conclusions

concerning the key role of low-lying multi-triplet bound states in determining the thermodynamic properties are summarized briefly in Sec. VI.

## II. FULLY FRUSTRATED LADDER

The frustrated Heisenberg spin ladder we consider is represented schematically in Fig. 1. In addition to the “rung” interaction,  $J_\perp$ , defining the fundamental dimer unit, and the “leg” interaction,  $J_\parallel$ , defining the two chains, we include a symmetrical cross-plaquette coupling,  $J_\times$ , which frustrates  $J_\parallel$ . The Hamiltonian of the model for any spin quantum number,  $S$ , and for a ladder of  $L$  rungs is

$$H = \sum_i J_\perp \vec{S}_i^1 \cdot \vec{S}_i^2 + \sum_{i,m=1,2} (J_\parallel \vec{S}_i^m \cdot \vec{S}_{i+1}^m + J_\times \vec{S}_i^m \cdot \vec{S}_{i+1}^{\bar{m}}), \quad (1)$$

where  $i$  is the rung index,  $m = 1$  and  $2$  denote the two chains of the ladder, and  $\bar{m}$  is the chain opposite to  $m$ . In our numerical calculations we will impose periodic boundary conditions, such that  $i + L \equiv i$ .

The primary focus of our investigation is the fully frustrated case,  $J_\times = J_\parallel$ . In this situation, the Hamiltonian (1) can be reexpressed in the form [47, 50]

$$H = J_\parallel \sum_{i=1}^L \vec{T}_i \cdot \vec{T}_{i+1} + J_\perp \sum_{i=1}^L \left( \frac{1}{2} \vec{T}_i^2 - S(S+1) \right), \quad (2)$$

where  $\vec{T}_i = \vec{S}_i^1 + \vec{S}_i^2$  is the total spin of rung  $i$  and  $S$  is the spin quantum number at each site. This expression makes clear that, for  $J_\times = J_\parallel$ , the Hamiltonian (1) has  $L$  purely local conservation laws, namely the total rung spin  $\vec{T}_i^2$ , which we may encode in additional quantum numbers  $T_i$ .

Although the form of Eq. (2) is valid for all  $S$ , we restrict our considerations henceforth exclusively to the case  $S = 1/2$ . Thus  $T_i$  takes the values 0 (a rung singlet, indicated by the ellipsoids in Fig. 1) or 1 (a rung triplet, represented by the two parallel rung spins in Fig. 1). For a given configuration  $\{T_i\}$ , the first term of Eq. (2) is finite only for groups of  $n$  neighboring rung triplets ( $T_i = 1$ ) with  $n \geq 2$ , in which case the Hamiltonian for the triplet cluster is that of an open  $n$ -site spin-1 chain. The second term in Eq. (2) is simply a number operator penalizing the presence of these rung triplets relative to rung singlets ( $T_i = 0$ ).

### A. Spectrum

#### 1. Ground State

As noted first in Ref. [45], the Hamiltonian (2) of the fully frustrated  $S = 1/2$  ladder [i.e. the model of Eq. (1) with  $J_\times = J_\parallel$ ] possesses a first-order quantum phase transition as a function of the coupling ratio  $J_\perp/J_\parallel$

[47, 50]. This transition separates a rung-singlet phase for strong  $J_\perp$  from a rung-triplet, or Haldane [3], phase at weak  $J_\perp$ . These two states have been found to dominate the phase diagrams of different generalized tetrahedral cluster models [48, 49, 51–59]. In the formulation of Eq. (2), the ground states are characterized by all  $T_i = 0$  ( $n = 0$ , rung-singlet phase) when  $J_\perp$  is dominant or all  $T_i = 1$  ( $n = L$ , Haldane phase) when the combination of  $J_\parallel$  and  $J_\times$  forces the creation of rung triplets to satisfy all of the inter-rung bonds. The ground-state energies are simply  $E_{n=0} = -\frac{3}{4} J_\perp L$  for the rung-singlet state and  $E_{n=L} = \frac{1}{4} J_\perp L + E_{S=1}(L)$  for the rung-triplet state, where  $E_{S=1}(L)$  is the ground-state energy of an  $L$ -site spin-1 chain with coupling constant  $J_\parallel$ . By using literature estimates [60, 61] for  $e_\infty = \lim_{L \rightarrow \infty} E_{S=1}(L)/L$ , the thermodynamic limit for the ground-state energy density of the spin-1 chain, one may conclude [45, 47, 50, 51] that the critical coupling constant for the quantum phase transition is

$$J_{\perp,c} = -e_\infty \approx 1.401484 J_\parallel. \quad (3)$$

With a view to discussing the thermodynamic properties of the fully frustrated ladder, in the remainder of this subsection we analyze the spin excitations above the two different ground states.

#### 2. Excited States of the Fully Frustrated Ladder and of Open Spin-1 Chains

The fundamental excitation of the rung-singlet state is a single rung triplet, represented schematically in Fig. 1. In conventional 1D systems, this is a collective mode involving all rungs, and for clarity we refer to it henceforth as the triplon. In the fully frustrated ladder, the triplon is a non-dispersive mode with a flat band at energy  $\omega_k = J_\perp$ . Further, it has been shown that the  $n$ -triplon clusters within the rung-singlet state form exact bound states [47], which are fully localized objects [45], and therefore are also non-dispersive. Thus one obtains an entirely discrete spectrum composed of the levels of  $n$ -site open Haldane chains, separated by an additional constant for the total  $n$  of the cluster; the case  $n = 2$  is discussed in Ref. [47]. In the rung-triplet phase, the ground state of the Haldane chain is known to be a total singlet with complex, system-scale spin entanglement quantified by the string-order parameter and dispersive triplet excitations with a gap  $\Delta = 0.4105 J_\parallel$  [60, 61]. These collective modes can be expected in the fully frustrated ladder to be accompanied by local excitations due to clusters of rung singlets in the triplet background.

We begin a quantitative discussion of the excitations by showing in Fig. 2 the complete low-energy spectrum of a fully frustrated 14-rung ladder, with  $J_\times = J_\parallel = 1$  as the unit of energy and  $J_\perp$  as the variable parameter. This figure was obtained from a full diagonalization, which is described in detail in Sec. III A. Here the rung-triplet phase is on the left side, the rung-singlet one is on the

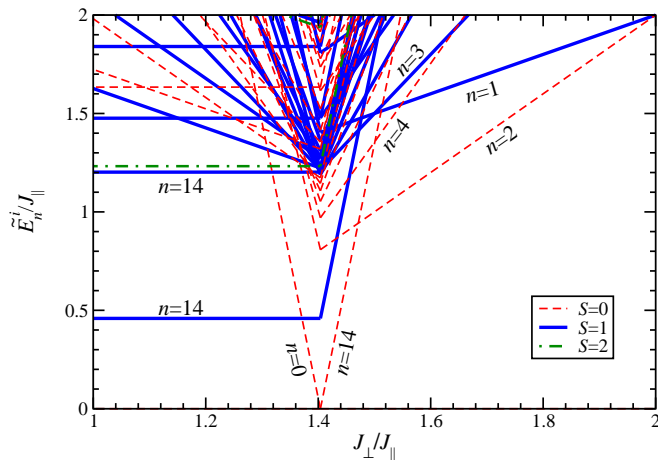


FIG. 2. (Color online) Low-energy excited levels,  $\tilde{E}_n^i$ , of a 14-rung fully frustrated spin-1/2 ladder, shown as a function of  $J_\perp/J_\parallel$ . All excitations are classified according to their total spin quantum number,  $S$ , and some by an additional label for the number,  $n$ , of consecutive rungs in the triplet state.

right, and the excitation energies,  $\tilde{E}_n^i$ , are the energy differences with respect to the corresponding ground state. We classify all the states in Fig. 2 by their total spin,  $S$ , and find only states with  $S \leq 2$  in the energy range covered by the figure, of which just three, all at high energies, are  $S = 2$ . We also label some of the states by the number  $n$  of consecutive triplet rungs ( $T_i = 1$ ) and comment that those states containing a single cluster with  $n < L$  consecutive rung triplets are  $L$ -fold degenerate, because they may be placed on the ladder in  $L$  possible ways.

$n$	spin	$S$	$E_{S=1}^i(n)/J_\parallel$	$n$	spin	$S$	$E_{S=1}^i(n)/J_\parallel$	
1	1		0	7	1		-8.634532	
2	0		-2	8	0		-8.303576	
	1		-1		0		-10.124637	
	2		1		1		-9.922759	
3	1		-3	9	1		-11.432932	
	0		-2		0		-11.220229	
	1		-1		10	0		-12.894560
	2		-1			1		-12.756229
4	1		0	11	1		-14.230359	
	2		1		0		-14.088587	
	3		2		12	0		-15.674010
	0		-4.645751			1		-15.576869
	1		-4.136582			13	1	
5	1		0		-16.931557			
5	0		-5.830213	14	0		-18.459853	
	0		-5.283567		1		-18.390687	
	6	0			$L$	0		$(-1.401484 \dots) L$

TABLE I. Energies  $E_{S=1}^i(n)$  of open, length- $n$ , spin-1 chains with exchange constant  $J_\parallel$ , classified by their total spin,  $S$ , and labelled by their different levels,  $i$ , in ascending order of energy. The value listed for  $n = L$  is an extrapolation to the thermodynamic limit, where the boundary conditions of the calculation are irrelevant.

For the interpretation of Fig. 2, in Table I we show the energies of various multiplets found in the spectrum of open,  $n$ -site, spin-1 chains for all values of  $n$  up to 14. The table is complete up to  $n = 3$ , beyond which we quote only the lowest states,  $i = 1$  and 2. As noted above, some of this information is available in the literature for  $n \leq 2$  [47] and for certain other energy differences [62]. Using the Hamiltonian in the form of Eq. (2), the energy of a single  $n$ -site, spin-1 cluster embedded in a fully frustrated  $L$ -rung ladder is

$$E_n^i = E_{S=1}^i(n) + (n - \frac{3}{4}L) J_\perp, \quad (4)$$

from which it is clear that many (but not all) of the lines in Fig. 2 may be identified by their slope and from the data of Table I.

Inspection of Table I reveals that the lowest states of open spin-1 chains have total spins  $S = 0$  and 1; when  $n$  is odd, the lowest-energy state is  $S = 1$ , whereas for  $n$  even, it has  $S = 0$ . This result may be understood in terms of the valence-bond-solid picture [63] of the Haldane phase, where the open chain ends give rise to effective  $S = 1/2$  spins unable to form valence bonds. These end spins experience an effective interaction, mediated by the “bulk” of the chain, which depends on the Hamiltonian and, for the Heisenberg chain, is such that the singlet state of the two end spins is lower in energy for  $n$  even, i.e. their effective interaction is antiferromagnetic, whereas for  $n$  odd the triplet is lower and the interaction ferromagnetic [62]. To display this result in a different perspective, in Fig. 3 we show for  $n \leq 20$  the energies  $E_{S=1}^i(n) - n e_\infty$  of the two lowest states of an open,  $n$ -site, spin-1 Heisenberg chain relative to the energy of the corresponding segment of an infinite chain. For the fully frustrated ladder, this quantity gives the excitation energy of a length- $n$  triplet segment in a background of rung singlets at the transition point,  $J_{\perp,c}$  (3), and one observes many of the levels of the discrete spectrum making the most important contributions to the physical properties of the system.

Figure 3 also displays the valuable information that the cost of breaking one bond in an infinite spin-1 Heisenberg chain is

$$E_{\text{bond}} = \lim_{n \rightarrow \infty} (E_{S=1}^i(n) - n e_\infty) \approx 1.208 J_\parallel, \quad (5)$$

but that interactions between the two effective end spins lead to significant lowering of this energy when the chain segment (triplet cluster) is short.

### 3. Excitations in the Rung-Singlet Phase

The information contained in Figs. 2 and 3 and in Table I may be used to provide a complete discussion of the low-energy excitations of the rung-singlet regime,  $J_\perp \geq J_{\perp,c}$ . First we comment that the lowest-lying state visible in Fig. 2 on this side of the transition, the  $S = 0$  state with  $n = 14 = L$ , is in fact a finite-size effect. This is the Haldane ground state at  $J_\perp \leq J_{\perp,c}$ , which has an

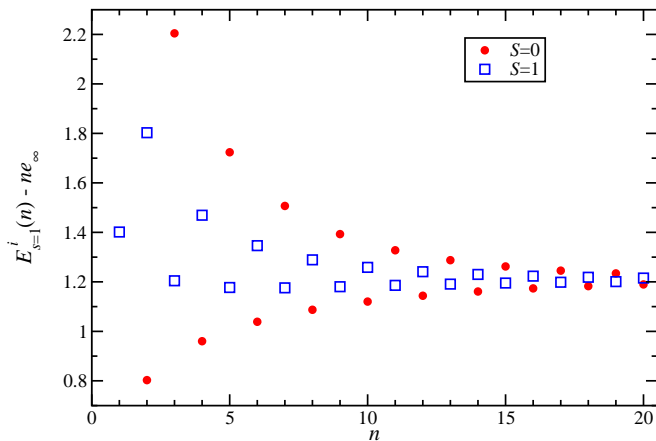


FIG. 3. (Color online) Energies of the two lowest states of an open,  $n$ -site, spin-1 Heisenberg chain relative to that of an  $n$ -site segment of an infinite chain, shown as a function of  $n$  and in units of  $J_{\parallel}$ . Red circles denote total singlets ( $S = 0$ ) and open blue squares total triplets ( $S = 1$ ).

energy proportional both to the distance from the transition point and to the system size. In the thermodynamic limit, its energy for any value  $J_{\perp}$  in the rung-singlet phase is infinite and it has no effect on the physical properties.

The energies of all the other states in Fig. 2 depend not on the system size but the cluster size, and these remain low-energy excitations in the thermodynamic limit. For  $J_{\perp} > 2J_{\parallel}$ , the lowest excitation is a single rung triplet ( $n = 1$ ), which has energy  $J_{\perp}$ , can be created on any rung, and creates the non-dispersive one-triplon band. At  $J_{\perp} \leq 2J_{\parallel}$  (the right boundary of Fig. 2), the  $S = 0$  branch of the two-triplon bound state ( $n = 2$ ), with a relative energy obtained from Eq. (4) of  $\tilde{E}_2^1 = E_2^1 + \frac{3}{4}J_{\perp}L = 2J_{\perp} - 2J_{\parallel}$ , lies lowest, and remains so until the transition, where its gap is approximately  $0.803 J_{\parallel}$  (cf. Ref. [47]). In this regime of  $J_{\perp}$ , the total singlet ( $S = 0$ ) of the ( $n = 4$ )-triplon bound state crosses the one-triplon state at  $J_{\perp} \simeq 1.55 J_{\parallel}$ , as may also be observed in Fig. 2. Next, the total triplet ( $S = 1$ ) level of the 3-triplon bound state, which is the lowest branch of this cluster (Fig. 3 and Table I) crosses at  $J_{\perp} \simeq 1.5 J_{\parallel}$ , on its way to an energy  $\tilde{E}_3^1 \simeq 1.204 J_{\parallel}$  at the transition. In fact the lowest magnetic excitation at  $J_{\perp} = J_{\perp,c}$  is the  $S = 1$  branch of the  $n = 5$  bound state, which has a gap  $\tilde{E}_5^1 \simeq 1.18 J_{\parallel}$  there. Thus the triplet gap is almost 50% larger than the singlet gap at the transition.

From the standpoint of discussing thermodynamic properties close to the quantum phase transition, the most important point in Fig. 2 is the fact that many further states with  $S = 0$  and 1 fall below the one-triplon gap as  $J_{\perp} \rightarrow J_{\perp,c}$ . These are the lowest-lying states of  $n$ -triplon clusters with all higher values of  $n$ , and their energies exactly at  $J_{\perp} = J_{\perp,c}$  are shown in Fig. 3. As  $n \rightarrow \infty$ , these energies converge to the value  $E_{\text{bond}} \approx 1.208 J_{\parallel}$  discussed in Eq. (5). The rung-singlet phase in the regime close to the transition is therefore

characterized by a very large number of states, of many-triplon origin, whose energies lie close to  $E_{\text{bond}}$ , accompanied by some few-triplon bound states providing levels, predominantly singlets, at lower energies.

#### 4. Excitations in the Rung-Triple Phase

In the rung-triplet (Haldane) phase at  $J_{\perp} \leq J_{\perp,c}$ , again the ground state of the rung-singlet phase appears in Fig. 2 as a finite-size effect when  $J_{\perp} \rightarrow J_{\perp,c}$ . This total singlet, labelled with  $S = 0$  and  $n = 0$ , again has a slope proportional to  $L$  and should be discounted in discussing the infinite system. Horizontal lines in Fig. 2 are states with all  $n = L = 14$  rungs in a spin triplet, and it is clear that not many such states with energies below  $2J_{\parallel}$  exist for this system size. The lowest of these lines, located at  $\tilde{E}_{14}^1 = E_{14}^1 - \frac{1}{4}J_{\perp}L \simeq 0.46 J_{\parallel}$ , is a total-spin triplet ( $S = 1$ ) and corresponds to the “one-magnon” Haldane gap [3] for  $L = 14$ ; as noted above, the value of this gap in the thermodynamic limit is  $\Delta \simeq 0.4105 J_{\parallel}$  [60, 61]. The Haldane chain is also known to have two-magnon scattering states with total spins  $S = 0, 1$ , and 2, which set in above the threshold energy  $2\Delta \simeq 0.821 J_{\parallel}$ . However, the lowest  $S = 2$  state for  $L = 14$  (Fig. 2) is found at  $\tilde{E}_{14}^2 \simeq 1.23 J_{\parallel}$  and the lowest  $S = 0$  state at  $\tilde{E}_{14}^5 \simeq 1.63 J_{\parallel}$ , showing that these extended (collective) features of the spectrum in the rung-triplet phase are subject to significant finite-size effects.

By contrast, the spectrum for  $J_{\perp} \leq J_{\perp,c}$  also contains levels with  $S = 0$  or 1 and a non-zero slope in Fig. 2. These features are the energy branches of rung-singlet clusters ( $T_i = 0$ ) in a background of rung triplets ( $T_i = 1$ ). Here the rung-singlet number is  $L - n$ , with  $n$  rung triplets, and the dominant features are those with small  $L - n$  ( $n$  approaching  $L = 14$ ); as  $n$  increases, the energies at  $J_{\perp,c}$  follow exactly the size-dependence shown in Fig. 3, converging for large clusters on the value  $E_{\text{bond}}$  (5). Thus, as on the rung-singlet side, the rung-triplet phase in the regime near the transition is dominated by a very large number of states appearing around a single, fixed energy close to (but above) the gap.

#### 5. Summary of the Low-Energy Spectrum

A summary of the previous two subsections for the spectrum of the fully frustrated ladder in the thermodynamic limit is provided in Fig. 4. In the rung-singlet phase ( $J_{\perp} > J_{\perp,c}$ ), the spectrum is purely discrete, with multiple low-energy branches appearing well below the one-triplon gap as  $J_{\perp} \rightarrow J_{\perp,c}$ . These have their origin in some of the shortest clusters, in particular the  $S = 0$  component of the two-triplon bound state, which provides the lowest excited state over the entire region  $J_{\perp,c} < J_{\perp} < 2J_{\parallel}$ .

In the rung-triplet phase ( $J_{\perp} < J_{\perp,c}$ ), the lowest-lying

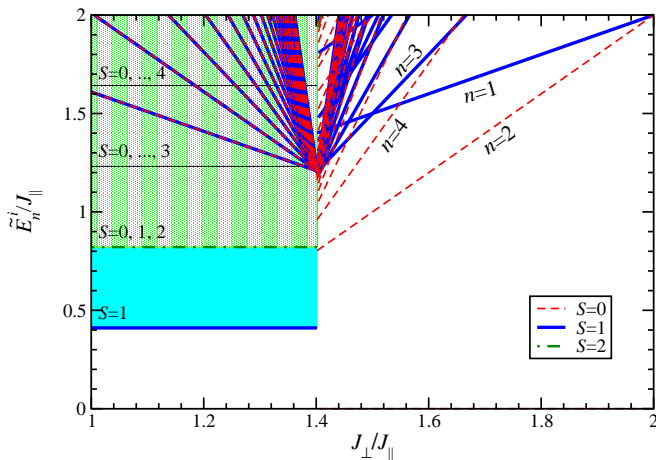


FIG. 4. (Color online) Schematic overview of the low-energy excitations,  $\tilde{E}_n^i$ , of the infinite, fully frustrated spin-1/2 ladder, shown as a function of  $J_{\perp}/J_{\parallel}$  for a broad region around the quantum phase transition at  $J_{\perp,c} = 1.410484$ . Excitations are classified according to their total spin quantum number,  $S$ . The additional label  $n$  for the rung-singlet phase specifies the origin of excitations in the bound states of  $n$ -rung triplets. Shaded regions in the rung-triplet phase denote single- and multiple-magnon continua.

modes are the dispersive single- and multi-magnon bands of the Haldane chain. The one-magnon band begins at a threshold  $\Delta$  and consists only of  $S = 1$  excitations. The two-magnon band has a threshold of  $2\Delta$  and gives rise to additional  $S = 0$  and  $2$  excitations. Two further thresholds fall within the energy range of Fig. 4 and are indicated by thin horizontal lines; at the three-magnon threshold,  $3\Delta$ , the first excitations with total spin  $S = 3$  appear, and similarly at  $4\Delta$ . The spectrum contains additional discrete (non-dispersive) energy levels due to excited rung singlets or rung-singlet clusters; increasingly long clusters provide low-lying levels as the transition is approached. As  $J_{\perp} \rightarrow J_{\perp,c}$ , all of the discrete excitations converge with increasing  $n$  to a single energy,  $E_{\text{bond}}$ , and are fourfold degenerate because the energies of the total  $S = 0$  and  $1$  states of the two effective end spins converge as their interaction vanishes.

To understand the densities of excited states in Fig. 4, we appeal again to finite ladders. Excitations arising from one cluster of rung triplets (singlets) in a background of singlets (triplets) are all  $L$ -fold degenerate for an  $L$ -rung system. Because there are  $L$  such states,  $L^2$  excitations have energies that converge to  $E_{\text{bond}} \simeq 1.208 J_{\parallel}$  at the critical point, and this is identical to the finite-size properties of a two-particle continuum. In the rung-triplet phase, the energy  $E_{\text{bond}}$  lies just below the three-particle threshold. However, we comment that the one-magnon band of the Haldane chain extends up to an energy of approximately  $6\Delta$  [60], which is beyond the range of Fig. 4, and thus the two-magnon continuum, extending to  $12\Delta$ , includes many states lying far above the energies of the discrete levels close to  $J_{\perp,c}$ . Thus

we expect the discrete levels to provide important contributions to the thermodynamic properties of the fully frustrated ladder for all values of  $J_{\perp}$  falling within the range of Figs. 2 and 4, not only on the rung-singlet side but also on the rung-triplet side, even if they are not the lowest-energy excitations. We analyze these contributions in Subsecs. II B and V A by considering short clusters and in Subsec. V B by considering a domain-wall description.

## B. Analytical Thermodynamic Approximations

To gain some initial insight into the effects of its unconventional spectrum on the thermodynamic properties of the fully frustrated ladder, in this section we consider a straightforward analytical approximation. Based on the exact  $n$ -triplon bound states of the rung-singlet phase ( $J_{\perp} > J_{\perp,c}$ ), we construct the partition functions of  $n$ -rung clusters and use them to obtain the magnetic specific heat, which we denote simply by  $C(T)$ , and magnetic susceptibility,  $\chi(T)$ , for ladder segments of increasing  $n$ . These results can also be compared with the analogous quantities computed for an unfrustrated ladder ( $J_{\times} = 0$ ) in the regime of strong  $J_{\perp}$  to observe the wider implications of strong frustration. For the purposes of this analysis, which we apply only in the rung-singlet regime, it is convenient in this subsection to normalize the energy scales of the system to the rung coupling,  $J_{\perp}$ .

The partition function of a single rung,  $Z_1$ , reflects the four available states, namely the singlet and three triplon components. That for a pair of rungs,  $Z_2$ , contains in place of the nine possible states of two separate triplons the nine levels of the total  $S = 0, 1$ , and  $2$  branches of the two-triplon bound state. By continuing in this way for the three-triplon bound states of a three-rung cluster, one obtains

$$\begin{aligned} Z_1(\beta) &= 1 + 3e^{-\beta J}, \\ Z_2(\beta) &= 1 + 6e^{-\beta J} + \sum_i g_2^i e^{-\beta \tilde{E}_2^i}, \\ Z_3(\beta) &= 1 + 9e^{-\beta J} + 3 \sum_i g_2^i e^{-\beta \tilde{E}_2^i} + \sum_i g_3^i e^{-\beta \tilde{E}_3^i}, \end{aligned} \quad (6)$$

where  $\beta = 1/T$  (we set  $k_B = 1$ ) and  $g_2^i$  and  $g_3^i$  are respectively the degeneracies of the different multiplets of the two- and three-triplon bound states, whose energies are  $\tilde{E}_2^i$  and  $\tilde{E}_3^i$  in the notation of Sec. II A. Note that the combinatorial factor in the expression for  $Z_3$  assumes that two-triplon bound states are formed for all possible pairs of triplon locations, implying that the boundary conditions of the three-rung cluster are periodic rather than open, and we will not differentiate between these cases for the approximate purposes of the current analysis. In the presence of a magnetic field,  $h = g\mu_B H$ , each multiplet is split into all of its separate levels, replacing  $g_n^i$  in Eq. (6) by factors of the form  $1 + 2 \cosh(\beta h) + 2 \cosh(2\beta h) + \dots$

The magnetic specific heat is obtained from the free energy,  $F = -\beta^{-1} \ln Z$ , using the expression

$$C(T) = -\frac{T}{V} \frac{\partial^2 F(T, h)}{\partial T^2} = \frac{\beta^2}{V} \frac{\partial^2 \ln Z(\beta)}{\partial \beta^2} \quad (7)$$

and the magnetic susceptibility using

$$\chi(T) = -\lim_{h \rightarrow 0} \frac{1}{V} \frac{\partial^2 F(T, h)}{\partial h^2} = \lim_{h \rightarrow 0} \frac{1}{\beta V} \frac{\partial^2 \ln Z(\beta, h)}{\partial h^2}. \quad (8)$$

$V$  is the system volume and here we use the number of sites,  $V = 2L$ , quoting all our results per spin-1/2 entity.

The construction of Eq. (6) forms a systematic basis for adding the effects of four- and higher-rung triplon clusters to investigate their contributions to the thermodynamic properties. Below we will also consider the thermodynamic quantities derived from  $Z_4$ , whose multiplet energies,  $\tilde{E}_4^i$ , were obtained from the spectrum of the four-site open Haldane chain (Table I). This method is readily continued to larger values of  $n$  and its efficacy will be compared with our numerical solutions in Sec. IV.

Here we focus on the qualitative properties of the specific heat and susceptibility, specifically their shape and evolution with the parameters of the ladder. We define the quantity  $j' = J_{\parallel}/J_{\perp}$  and consider fully frustrated ladders ( $J_{\times} = J_{\parallel}$ ) for all values  $0 \leq j' \leq 0.71$  within the rung-singlet phase. The thermodynamic properties of the frustrated ladder may be benchmarked against those of the unfrustrated two-leg spin ladder. These we also calculate by an approximate method, using the bond-operator mean-field technique with Ansatz hardcore-boson triplet statistics and no higher-order correlations, following Ref. [64]. This approach approximates the shifts of spectral weight at finite temperatures by a single, effective one-triplon band, which remains sharp rather than including thermal broadening. As a result, it is known to overestimate the thermal band-narrowing effect, whence the neglect of further correlations (which exacerbate this effect). This approximation has been found to give an excellent account of the gap and band width of the unfrustrated ladder over the parameter range  $0 \leq j' \leq 1$ , which exceeds the regime of the current investigation.

Results for the specific heat of unfrustrated ladders and of frustrated ladders computed using  $Z_2$ ,  $Z_3$  [Eq. (6)], and  $Z_4$  are shown in Fig. 5 for a range of coupling ratios,  $j' = J_{\parallel}/J_{\perp}$ , in the rung-singlet phase. The common feature of every panel is the curve for  $j' = 0$ , the specific heat (per spin) of an isolated ladder rung,

$$C_r(T) = \frac{3(\beta J_{\perp})^2 e^{-\beta J_{\perp}}}{2(1 + 3e^{-\beta J_{\perp}})^2}, \quad (9)$$

which shows an exponential increase at low temperature characteristic of a gap  $\Delta = J_{\perp}$ , a maximum at  $T = 0.35J_{\perp}$ , and a power-law decay towards higher temperatures. The results for the unfrustrated ladder in Fig. 5(a) show that, as the leg coupling  $J_{\parallel}$  is increased,

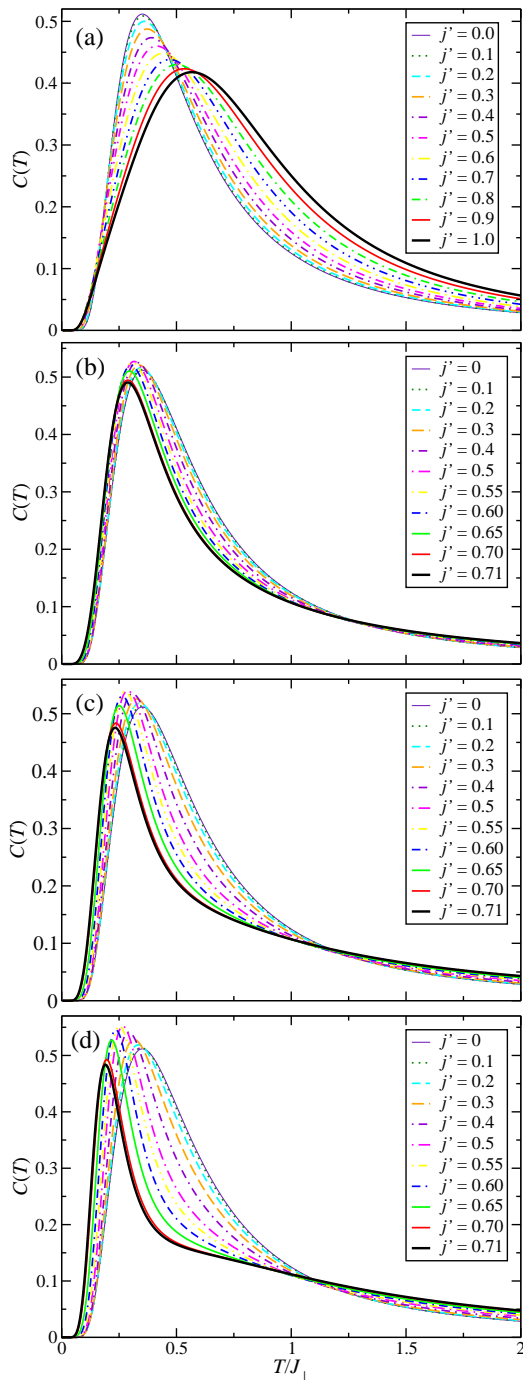


FIG. 5. (Color online) Magnetic specific heat of (a) the unfrustrated ladder, (b) two, (c) three, and (d) four fully frustrated rungs, shown as functions of temperature for a range of values of the inter-rung coupling,  $j' = J_{\parallel}/J_{\perp}$ .

the increasing triplet band width causes a slow but continuous reduction of the gap and a shift of weight to higher energies. The specific-heat maximum displays a monotonic decrease in its height,  $C_{\max}$ , but an increase in the temperature,  $T_{\max}^C$ , at which it occurs, as  $j'$  increases. We stress that this calculation shows only the

contributions of the one-triplon excitations, whose density of states is concentrated between a gap  $\Delta$ , which drops from  $J_\perp$  at  $j' = 0$  to approximately  $J_\perp/2$  at  $j' = 1$  [65, 66], and an upper edge close to  $J_\perp + 2J_\parallel$ . However, because the maximum in  $C(T)$  already increases with  $j'$  for the single-band contribution, we expect that multi-triplon contributions, which appear at higher temperatures, can only strengthen this effect.

In the fully frustrated ladder, the evolution of the specific heat is quite different. For the two-rung approximation [Fig. 5(b)],  $T_{\max}^C$  does not rise with the coupling but instead is suppressed monotonically in temperature by increasing  $j'$ . This is not a consequence of changes in the gap, as  $\Delta$  begins to drop only beyond  $j' = 0.5$  (Sec. II A).  $C_{\max}$  first increases weakly with  $j'$ , to a maximum value at  $j' = 0.5$ , before falling somewhat more rapidly as  $j' \rightarrow j'_c$ . The three-rung approximation, shown in Fig. 5(c), exaggerates these tendencies, and the four-rung approximation exaggerates them still further [Fig. 5(d)], meaning that the strongest alterations visible due to including larger  $n$ -triplon clusters occur for the coupling values closest to the transition.

We draw three conclusions from the specific heat. First, its behavior as a function of  $j'$  in the fully frustrated ladder is completely different from that of the unfrustrated ladder over the whole range of  $j'$ . Second, even the two-rung approximation may already capture the basic phenomenology of bound-state effects, although additional bound states are responsible for strengthening these effects, which are most pronounced close to the quantum phase transition at  $j'_c$ . Third, the peak of the specific heat becomes significantly smaller (narrower as well as lower) as  $j \rightarrow j'_c$ , with very little weight moving to lower energies due to the (weakly) decreasing gap; clearly most of the “missing” entropy caused by the peak suppression near  $j'_c$  is retrieved at higher temperatures, beyond the apparent crossing point of the curves at  $T \approx J_\perp$ . Thus despite the fact that the one-triplon band is completely flat and the leading effect of bound-state formation to produce a sharper peak at lower energies, one overall effect of the frustrated coupling is to push the available states to a higher average energy.

The corresponding susceptibilities per spin are presented in Fig. 6, where we show only the four-rung approximation for the fully frustrated ladder. Again the two panels are anchored by the  $j' = 0$  result, the susceptibility,

$$\chi_r(T) = \frac{\beta e^{-\beta J_\perp}}{(1 + 3e^{-\beta J_\perp})}, \quad (10)$$

of an isolated spin-1/2 dimer with coupling constant  $J_\perp$  [67–69], which is activated at low  $T$  by the gap  $\Delta = J_\perp$ , has a broad peak at approximately  $T = 0.62J_\perp$ , and falls very slowly to high temperatures. The susceptibility of the unfrustrated ladder [Fig. 6(a)] has the same basic features as the specific heat [Fig. 5(a)], namely that the gap determining the low- $T$  response decreases steadily with  $j'$  but the peak position,  $T_{\max}^\chi$ , increases, although

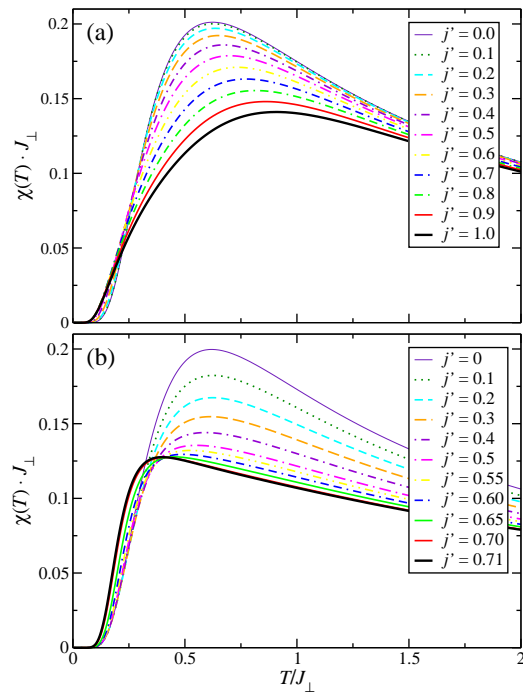


FIG. 6. (Color online) Magnetic susceptibility of (a) the unfrustrated ladder and (b) the four-rung approximation to the fully frustrated ladder, shown as functions of temperature for a range of values of the inter-rung coupling,  $j' = J_\parallel/J_\perp$ .

its height,  $\chi_{\max}$ , falls. The two quantities  $C$  and  $\chi$  are always characterized by the same gap.

The susceptibility of the fully frustrated ladder [Fig. 6(b)] is again quite different from the unfrustrated case, but not particularly similar to the specific heat [Fig. 5(d)].  $T_{\max}^\chi$  barely moves with  $j'$  until  $j' > 0.3$ , then moves increasingly rapidly to lower temperatures;  $\chi_{\max}$  does fall with  $j'$  but then changes very little as  $j'$  approaches  $j'_c$ . We remind the reader that, while  $C$  is the response due to all excited states,  $\chi$  is the response due only to all excited magnetic states, and thus the gap to triplet and higher-spin excitations is constant ( $\Delta^\chi = J_\perp$ ) for all values of  $j'$  except for a small drop over the range  $2/3 \leq j' \leq j'_c$ , ending at  $\Delta_c^\chi = 0.857J_\perp$ . Thus we have the situation that  $\chi$  is not characterized by the same gap as  $C$ , which is quite unusual in magnetic systems and is another consequence of the strong frustration.

The susceptibilities calculated using  $Z_2$  and  $Z_3$  (not shown here, but presented for selected  $j'$  values in Sec. V A) display the same trend towards the features of the  $Z_4$  result as do the cruder approximations to the specific heat (Fig. 5). Again one may conclude that very small numbers of bound states are sufficient to capture all the features of the thermodynamic response when  $j'$  is far from  $j'_c$  in the rung-singlet phase. We will quantify this statement by comparison with our numerical results in Sec. V, where we will find that the four-rung approximation of Figs. 5(d) and 6(b) already achieves quantitative accuracy for  $j' \leq 0.5$ , i.e. contributions from  $n$ -triplon

clusters with  $n > 4$  are negligible in this regime. The crucial effects of bound-state formation in the fully frustrated ladder that we wish to investigate with our advanced numerical techniques are those occurring in the vicinity of the quantum phase transition, and thus in Secs. III and IV we will focus on the parameter range  $0.5 \leq j' \leq 1$  shown in Figs. 2 and 4.

### III. NUMERICAL METHODS

The Hamiltonian of the fully frustrated ladder expressed in the rung basis of Eq. (2) is particularly valuable from a numerical standpoint. In this section we explain the methods we apply both to extend ED calculations to larger system sizes and to perform sign-problem-free QMC simulations even for a highly frustrated system. Readers not interested in the technical details of these approaches may continue directly to the results presented in Sec. IV.

#### A. Exact Diagonalization

The model specified in the form (2) has a large number of sectors classified by the fixed set of rung quantum numbers  $\{T_i\}$ ,  $i = 1, \dots, L$ , and each sector may be diagonalized separately. Further, as explained in Sec. II A, every sector can be characterized entirely by either the spectrum of a periodic,  $L$ -site, spin-1 chain (if all rungs are in a triplet state) or the spectrum of open,  $n$ -site, spin-1 chains for all  $n$ -triplon clusters with  $n < L$ . The complete spectrum is constructed by considering the combinatorial factors obtained by embedding all such open chain segments into the ladder and counting the (discrete) energy levels that appear with their corresponding multiplicities.

For the two cases where  $T_i = 0$  for all  $i$  (rung-singlet phase) or  $T_i = 1$  for all  $i$  (rung-triplet), there is only one such possibility. Single chain segments, of any  $n$ , may be embedded at  $L$  places and therefore the energies (4) are  $L$ -fold degenerate (Sec. II). For general numbers of chain segments, of different lengths and positions on the ladder, the combinatorial factors are enumerated by computer. The key physical property allowing such a straightforward approach is that the interaction between any two neighboring singlet and triplet rungs (and indeed between two singlet rungs) is precisely zero, so that rung and cluster states need only be placed side by side in all possible combinations. This type of strategy has been applied previously to models with local conservation laws [70–72], including to the fully frustrated ladder [70], where the calculations were restricted to systems up to  $L = 12$  (24 spins). Here we extend this treatment to  $L = 14$ , a value that we note lies beyond the limit of 24  $S = 1/2$  spins accessible in conventional full-diagonalization calculations, even for systems with high spatial symmetry [32].

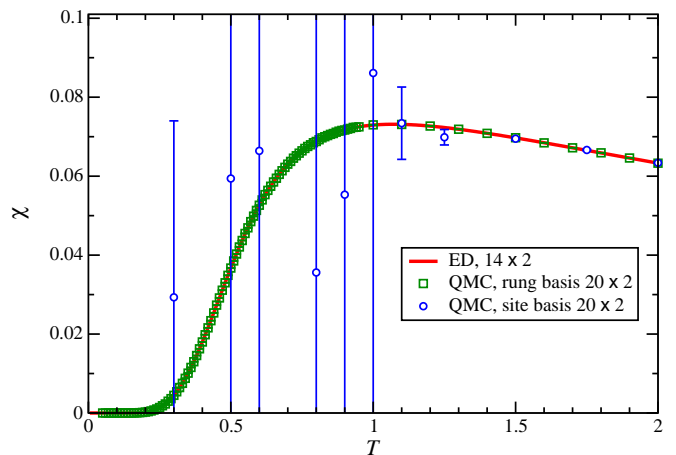


FIG. 7. (Color online) Comparison of the magnetic susceptibility,  $\chi$ , obtained for a fully frustrated ladder with  $J_{\perp} = 2$  and  $J_{\parallel} = J_{\times} = 1$ , between QMC results for a system of  $L = 20$  rungs and ED results for  $L = 14$ . QMC simulations were performed in both the single-site basis and the rung basis.

In the calculations presented here, we exploit spatial reflection symmetry and also translational symmetry for the periodic  $L$ -site  $S = 1$  system. We make use of the conservation of total  $S^z$ , of spin inversion symmetry, and of  $SU(2)$  symmetry in order to reconstruct the  $S^z = 1$  sector from the other sectors. The most demanding computation is the diagonalization of the open spin-1 chain with  $n = L - 1$  sites. For the  $L = 14$  ladder, the open spin-1 chain with  $n = 13$  sites (representing the contribution of 13-triplon clusters) has a vector-space dimension up to 85616 for  $S^z = 2$ . Results for the periodic  $L = 14$  spin-1 chain are in fact available from a previous investigation [43]. Beyond these full-diagonalization procedures, we have also computed the ground-state energies of open spin-1 chains with  $14 \leq n \leq 20$  sites using the Lanczos algorithm [73, 74]; these results are included in Fig. 3, and also in Table I for  $n = 14$ .

#### B. Quantum Monte Carlo

Calculations for the thermodynamic properties of all systems larger than those accessible by ED require a different numerical method. In 1D the primary options for general models are TMRG (Sec. I) and QMC, and here we employ the latter. QMC simulations of frustrated spin systems are well known to suffer from the notorious “sign problem,” where the statistical weights of the effective classical system may become negative. As an example we consider a conventional simulation of the fully frustrated ladder in the single-site basis of Eq. (1) using the stochastic series expansion (SSE) representation with directed loop updates [75]. Results for the susceptibility,  $\chi$ , of an  $L = 20$  ladder with  $J_{\perp} = 2J_{\parallel}$  are shown by the open (blue) circles in Fig. 7, where they are compared

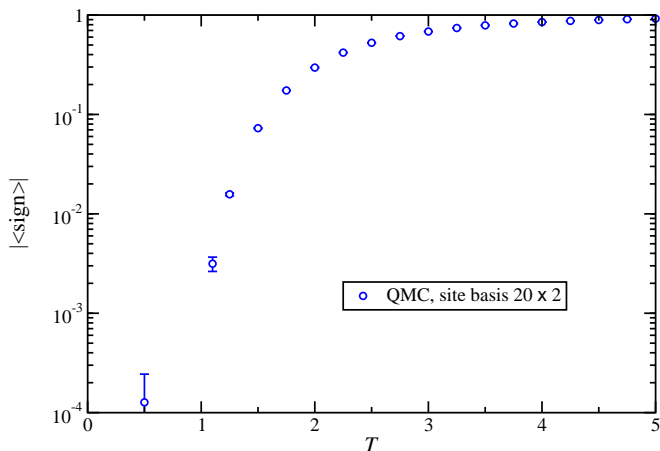


FIG. 8. (Color online) Average sign obtained during QMC simulations in the single-site basis of the  $L = 20$  ladder with  $J_{\perp} = 2$  and  $J_{\times} = J_{\parallel} = 1$ .

with ED results obtained for  $L = 14$ , a system size large enough to be considered representative of the thermodynamic limit for these parameters (as we show explicitly in Sec. IV). Clearly the QMC results obtained in the single-site basis are accurate only at high temperatures, but break down even on approaching the maximum of  $\chi$  at  $T \approx J_{\parallel}$ ; specifically, the error bars become so large that the maximum cannot be resolved.

This manifestation of the sign problem (Fig. 7) is presented in Fig. 8 in the form of the average sign,  $\langle \text{sign} \rangle$ , of the statistical weight obtained at different temperatures. At high  $T$  this is close to 1, whereas for temperatures  $T < 2J_{\parallel}$ , and particularly  $T < J_{\parallel}$ , it falls rapidly towards zero (note the logarithmic scale in Fig. 8). Only for  $T \gtrsim 1.5J_{\parallel}$  can accurate data be obtained, at a high cost in CPU time, but for temperatures  $T \lesssim J_{\parallel}$  the positive and negative contributions are so close in absolute value that the error in their difference can no longer be controlled. We comment that  $L = 20$  (Figs. 7 and 8) remains a comparatively small system, while the sign problem is known to scale exponentially in both system size and inverse temperature ( $\beta = 1/T$ ) [76].

However, the nature and severity of the sign problem depend on the basis in which the simulation is constructed. The fully frustrated ladder presents a particularly clear example where the Hamiltonian can be expressed not in the site basis of Eq. (1) but in the spin-dimer (rung) basis of Eq. (2). For a given rung  $i$ , we consider the local basis states

$$\begin{aligned}
 |S\rangle_i &= \frac{1}{\sqrt{2}}(|\uparrow\downarrow\rangle_i - |\downarrow\uparrow\rangle_i), \\
 |0\rangle_i &= \frac{1}{\sqrt{2}}(|\uparrow\downarrow\rangle_i + |\downarrow\uparrow\rangle_i), \\
 |+\rangle_i &= |\uparrow\uparrow\rangle_i, \\
 |-\rangle_i &= |\downarrow\downarrow\rangle_i.
 \end{aligned} \tag{11}$$

The idea of performing QMC simulations in a spin-dimer basis was suggested by Nakamura [77], who considered a

different basis, symmetric under spin reflection, which allowed him to simulate the  $J_1$ - $J_2$  Heisenberg spin chain over an extended parameter region. Here, however, the basis of Eq. (11) is more suitable because it makes the total dimer spin operators,  $T_i^z$ , diagonal and thus quantities such as the susceptibility are readily accessible.

The change of computational basis requires the simulation of composite-spin operators, i.e. updates of both quantum numbers  $T_i$  and  $T_i^z$ . The off-diagonal part of the Hamiltonian in the rung basis (2) can be decoupled in terms of the total-spin raising and lowering operators,  $T_i^{\pm}$ , and the SSE QMC method implemented with the standard diagonal update scheme [75]. Directed loop updates are implemented by employing the linear programming approach of Ref. [78] to solve the directed loop equations numerically in order to minimize bounces during the operator loop construction. We considered in particular the set of non-trivial permutations of the four spin-dimer basis states as local operators that are applied during the directed loop update. For this one may employ both the total-spin raising and lowering operators,  $T_i^{\pm}$ , and the raising and lowering operators  $D_i^{\pm}$ , constructed from the spin-difference operator  $\vec{D}_i = \vec{S}_i^1 - \vec{S}_i^2$ , combined with the local  $D_i^z$  operators. The latter are not diagonal in the spin-dimer basis. The action of the different operators on the local dimer basis states is shown in Table II.

When QMC simulations are performed in the spin-dimer basis, the sign problem is completely absent for an even number  $L$  of rungs. One may verify that the average sign computed in Fig. 8 is now identically equal to 1. This occurs because the chain of rung “super-sites” forms a bipartite lattice on which the exchange interactions between nearest-neighbor total spins ( $\vec{T}_i$ ) are bilinear (2). By using a similar amount of CPU time for simulations in the dimer basis as for the single-site basis, we now obtain the data shown by the open (green) squares in Fig. 7. The results resolve not only the maximum of  $\chi$  but also the complete low-temperature behavior all the way to  $T = 0$ . However, here we find a different consequence of the extensive number of local conservation laws in Eq. (2), namely that these hinder an effective mixing of the local spin states. As a result, the autocorrelation and thermalization times become very large at low temperatures and close to the quantum phase transition [Eq. (3)], requiring further modification of our approach.

	$\vec{T}_i^2$	$T_i^z$	$T_i^+$	$T_i^-$	$D_i^z$	$D_i^+$	$D_i^-$
$ S\rangle_i$	0	0	0	0	$ 0\rangle_i$	$-\sqrt{2} +\rangle_i$	$\sqrt{2} -\rangle_i$
$ 0\rangle_i$	2	0	$\sqrt{2} +\rangle_i$	$\sqrt{2} -\rangle_i$	$ S\rangle_i$	0	0
$ +\rangle_i$	2	1	0	$\sqrt{2} 0\rangle_i$	0	0	$-\sqrt{2} S\rangle_i$
$ -\rangle_i$	2	-1	$\sqrt{2} 0\rangle_i$	0	0	$\sqrt{2} S\rangle_i$	0

TABLE II. Action of local total-spin and spin-difference operators on the local spin-dimer basis states. Because  $\vec{T}_i^2$  and  $T_i^z$  are diagonal in this basis, we give only the eigenvalues for these operators.

To perform QMC simulations for suitably large system sizes under these circumstances, we employed a standard parallel tempering protocol [79–81] over a set of 64 temperatures, although 32 values were found to be sufficient at coupling ratios far from the phase transition. Each replica was passed through an initial annealing phase, where it was heated slowly from an appropriate low-temperature state to its target temperature. The simulations were initialized by taking as the SSE base state (with an empty operator string) a rung-singlet product state for  $J_{\perp}$  within the rung-singlet phase ( $J_{\perp} > J_{\perp,c}$ ) and an antiferromagnetic Néel state for  $J_{\perp}$  within the rung-triplet phase ( $J_{\perp} < J_{\perp,c}$ ). The parallel tempering swap rates were adapted to allow for sufficient autocorrelation of the replicas between swaps.

We comment here that a dimer-basis description appears natural for quantum magnets with a dimerization in their interaction geometry. The QMC simulation scheme presented here can be extended to the case of arbitrary spin systems whose interactions are bilinear when reexpressed in the basis of spin-dimer singlet and triplet states. In addition to interdimer exchange couplings based on  $\vec{T}_i$  operators, which we denote as  $TT$ -type terms, the most general case would also include couplings of  $DD$ ,  $TD$ , and  $DT$  types. For models with  $TT$  terms only, and for which the dimer super-sites form a bipartite lattice, the QMC sign problem is completely eliminated, as in the fully frustrated spin ladder. In fact all such models are strongly constrained by local conservation laws on every spin dimer, but any additional interaction terms break these laws explicitly. Local transitions then become possible between the singlet and triplet sectors, allowing for a more efficient mixing of states within QMC simulations, but at the price that such additional interaction terms lead generically to a QMC sign problem (even in the spin-dimer basis).

In Table II, we find that (i) the  $\vec{T}_i$  operators do not create transitions between singlet and triplet sectors and (ii) the  $D_i^z$  operators do swap local  $|S\rangle$  and  $|0\rangle$  states. In a model containing only  $TT$  and  $D^z D^z$  terms, and with a bipartite structure of couplings between dimers on different sublattices only, again the sign problem is completely absent, because the periodic boundary conditions in the discrete imaginary-time propagation direction mandate that only even numbers of interdimer  $D^z D^z$  terms can create allowed QMC configurations. All allowed configurations then contribute to the quantum partition function with positive weight (this is a straightforward generalization of the reason that no sign problem plagues world-line simulations of the antiferromagnetic Heisenberg model on a bipartite lattice) [82]. However, we note that in such a model  $SU(2)$  symmetry is broken explicitly.

These considerations highlight that special cases exist for particular subsets of interaction terms, which can be handled by QMC without generating a sign problem at all. For more general systems with dimerized ground states [70–72], the possibility arises that, even when non-positive QMC weights can occur, a simulation may have

only a mild QMC sign problem because the ground state is a direct product state (of dimer singlets). Further analysis to assess the full potential of the spin-dimer-based approaches to QMC lies beyond the scope of the current study. We highlight only one further extension of these ideas, to consider the construction of more general computational bases, formed from larger lattice units, or simplices, such as triangles [50] or four-site plaquettes [83]. The development of simplex-QMC methods to explore geometries and interactions providing sign-problem-free or sign-problem-suppressed simulations can be expected to provide valuable progress in frustrated quantum magnetism.

#### IV. THERMODYNAMIC PROPERTIES: NUMERICAL RESULTS

In this section we present our numerical results for the thermodynamic properties of the fully frustrated ladder and of some unfrustrated comparison cases. We begin by ensuring the accuracy and reliability of our calculations by comparing the results from ED and QMC, primarily to verify that finite-size effects are under control throughout the phase diagram, including in the vicinity of the critical point [Eq. (3)]. We present the basic phenomenology of the magnetic specific heat,  $C$ , and susceptibility,  $\chi$ , in terms of the physical features emerging as the interaction parameters are changed in two directions, from rung-singlet to rung-triplet ladders and from fully frustrated to unfrustrated ladders. Following the results of Sec. II B, we focus on the parameter regime  $1 \leq J_{\perp}/J_{\parallel} \leq 2$  around the phase transition. We defer to Sec. V a deeper analysis of our results and of their interpretation using the information about the spectrum presented in Sec. II A. However, for the most elementary understanding of the response functions it is worth recalling that the specific heat is a consequence of all states and therefore reflects primarily the singlet bound states in the vicinity of  $J_{\perp,c}$ , whereas the susceptibility is a consequence of all magnetic states and therefore reflects primarily triplet bound states.

##### A. Finite-Size Convergence: Comparison of ED and QMC

With a view to benchmarking the quality of our numerical calculations, Fig. 9 compares ED and QMC results for the specific heat and susceptibility of fully frustrated ladders with four different values of the ratio  $J_{\perp}/J_{\parallel}$ , selected in the rung-singlet phase far from  $J_{\perp,c}$ , in the rung-singlet phase close to  $J_{\perp,c}$ , and similarly in the rung-triplet phase. Every panel shows ED results calculated for ladders of 10, 12, and 14 rungs, along with QMC data for 100-rung ladders and additional QMC results from 200-rung ladders when  $J_{\perp}$  is close to  $J_{\perp,c}$ . Quite generally, all the susceptibility curves are nearly indis-

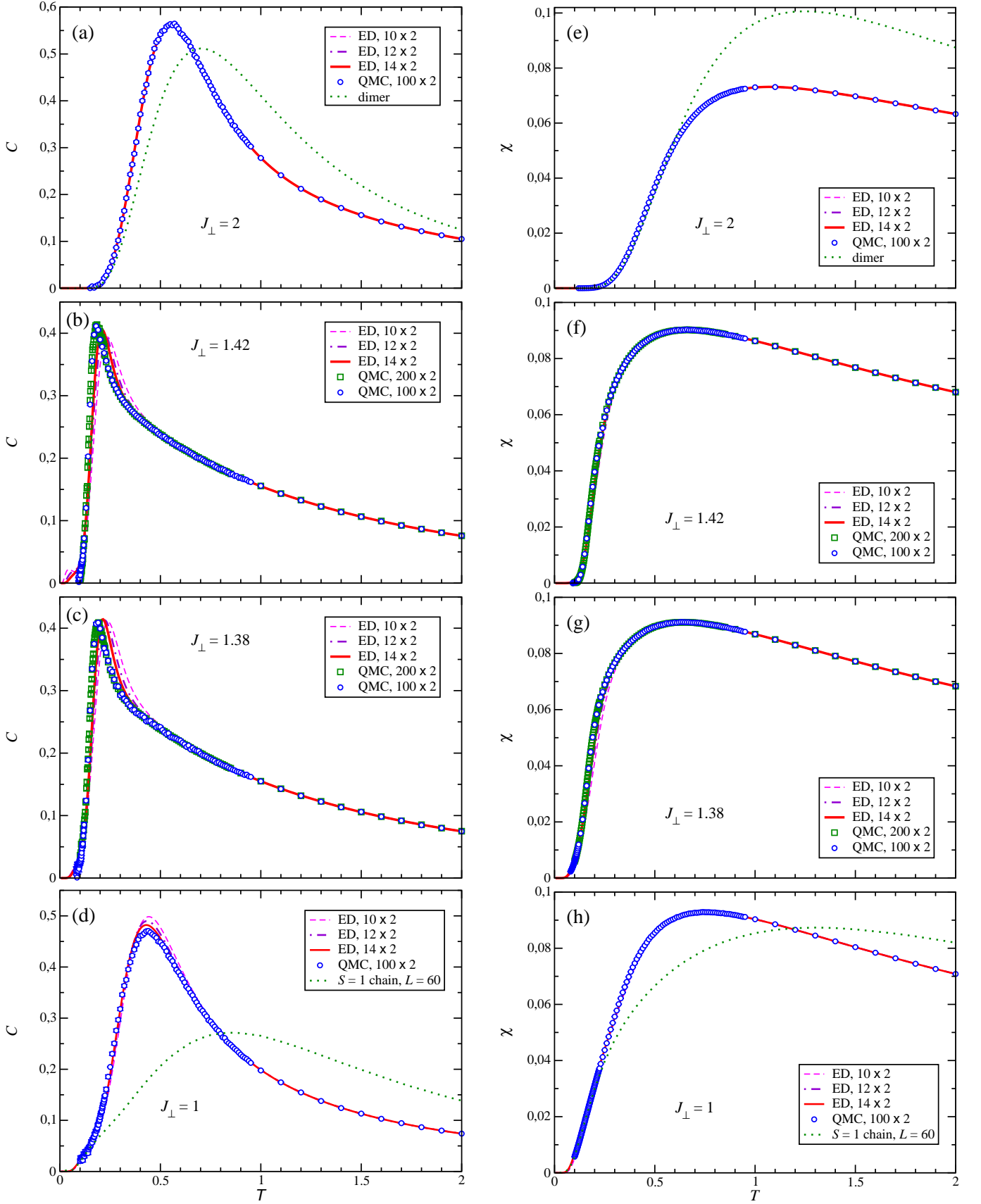


FIG. 9. (Color online) Specific heat,  $C$  (left column), and susceptibility,  $\chi$  (right column), per spin for fully frustrated ladders with inter-rung couplings  $J_x = J_{\parallel} = 1$  and rung couplings  $J_{\perp} = 2, 1.42, 1.38,$  and  $1$  (from top to bottom). Each panel compares ED results for system sizes of  $L = 10, 12,$  and  $14$  rungs with QMC results obtained for  $L = 100$  rungs. In panels (a) and (e) we include the results (9) and (10) for isolated dimers of rung coupling  $J_{\perp} = 2J_{\parallel}$ . In panels (d) and (h) we include QMC results for a spin-1 chain of  $L = 60$  sites [43], normalized to twice the number of spins in the chain.

tinguishable, meaning that finite-size effects in  $\chi$  are extremely small, and we focus most of our comments on the specific-heat results.

The fact that identical curves are obtained for the specific heat of the  $J_{\perp}/J_{\parallel} = 2$  ladder (top) indicates that a system with  $L = 10$  rungs can be considered as a good approximation to the thermodynamic limit. By contrast, finite-size effects are significantly more important at  $J_{\perp}/J_{\parallel} = 1.42$ , where there is a systematic shift of the peak to the left from  $L = 10$  to 12 to 14, and none of the ED calculations capture the peak position of the QMC results. Although this type of shift could be interpreted as reflecting the importance of longer clusters, in the same way as observed in Fig. 5, it may seem surprising that clusters of more than 10 rungs could make a discernible difference at  $|J_{\perp} - J_{\perp,c}|/J_{\parallel} \approx 0.02$ , given that the ground state is still a simple product of rung singlets. However, we recall that in systems of the sizes accessible by ED, the lowest excitation in this regime is actually the “intruder” state, which is the ground state on the rung-triplet side of the transition, as shown in Fig. 2 and discussed in Sec. II A, and this causes differences in the thermodynamic response. Here we also include QMC results for a ladder of  $L = 200$  rungs, and these make clear that all finite-size phenomena are thoroughly suppressed in our  $L = 100$  data.

Turning to the rung-triplet side of the transition, the same finite-size effects are visible at  $J_{\perp}/J_{\parallel} = 1.38$  as at 1.42; in fact they are slightly more pronounced, to the extent that they are visible in the corresponding curve for the susceptibility, where we draw attention to the different temperatures at the center of the rapid rise. Thus it is clear that the thermodynamic response of the Haldane phase close to the critical point is significantly affected by the intruding rung-singlet ground state. Whether large clusters (of rung singlets) or the one-magnon band of the Haldane chain play a role here is unclear. Moving well into the Haldane phase, at  $J_{\perp}/J_{\parallel} = 1$  we observe finite-size effects not in the position of the specific-heat peak at  $T \approx 0.5 J_{\parallel}$  but in its height. This type of size effect can be found in calculations of the Haldane (spin-1 Heisenberg) chain [43], and thus its appearance in the rung-triplet phase of the ladder suggest that it is due to long spin-1 chain segments separated by excited rung singlets. From our results and also from those for the Haldane chain, the QMC data for  $L = 100$  can be considered as fully converged to the thermodynamic limit for this choice of parameters. For thermodynamic purposes, we take finite-size effects to be negligible in the fully frustrated ladder of  $L = 100$  rungs for all values of  $J_{\perp}$ .

## B. Dependence of $C$ and $\chi$ on $J_{\perp}$

We turn now to a discussion of how the thermodynamic response of the fully frustrated ladder depends on the rung coupling ratio  $J_{\perp}/J_{\parallel}$ , continuing with accurate

numerical data from near the transition the investigation begun in the rung-singlet phase in Sec. II B. Considering again the sequence of panels in Fig. 9, at the top is the case  $J_{\perp} = 2 J_{\parallel}$ , representative of strong rung coupling. As in Sec. II B, we compare the specific heat and susceptibility with the results (9) and (10) for decoupled dimers ( $J_{\perp} \gg J_{\parallel}$ ), illustrated here for a bond strength  $J_{\perp} = 2$ . We observe again that, despite the formation of bound states at and above the one-triplon energy (Sec. II A), the leading effect of frustration is to push the maximum of the specific heat to a lower temperature and to make its peak higher and narrower than that of one dimer. The maximum of the susceptibility is also pushed to lower temperatures, although here the dominant effect is the suppression of the peak height compared with a single dimer (Sec. II B).

On proceeding towards the critical point (3), the maximum of the specific heat becomes progressively lower and narrower, developing a remarkably sharp profile close to  $J_{\perp,c}$ , as illustrated by the cases  $J_{\perp}/J_{\parallel} = 1.42$  and 1.38 in Fig. 9. We observe that the peak position falls by a factor of 3 from  $J_{\perp}/J_{\parallel} = 2$  to 1.42, while the gap, which is to the singlet branch of the two-triplon bound state, falls by a factor of 2.5 in units of  $J_{\parallel}$  (Subsec. II A and Fig. 4). This change of effective temperature scale is apparent also in the rise of the susceptibility, which we characterize by the temperature,  $T_{\text{half}}^{\chi}$ , where it has gained half of its peak height. In this case,  $T_{\text{half}}^{\chi}$  falls by a factor of 2.5 from  $J_{\perp}/J_{\parallel} = 2$  to 1.42 while the triplet gap falls only by 30%.

To study this evolution of the specific heat and susceptibility in more detail, Fig. 10 presents data for both quantities in contour form as a function of the coupling ratio,  $1 \leq J_{\perp}/J_{\parallel} \leq 2$ , and temperature,  $T$ . These results were obtained by exact diagonalization of a 14-rung ladder, where we recall (Subsec. IV A) that finite-size effects due to the intruder states (Fig. 2) occur near  $J_{\perp,c}$ . Indeed a very weak V-shaped feature is discernible in the specific heat at the lowest temperatures near  $J_{\perp} = 1.4 J_{\parallel}$ , but these effects remain so small for  $L = 14$  that the qualitative behavior is not affected. The quantum phase transition (3) is clearly visible as a dip in both thermodynamic quantities as a function of  $J_{\perp}/J_{\parallel}$ . This dip is more apparent, and more symmetrical, in the specific heat than in the susceptibility. The energy and temperature scales marked by the lines in Fig. 10 as an aid to characterizing the positions and widths of the peaks in  $C$  and  $\chi$  are discussed in detail in Sec. V.

For a fully quantitative investigation of the thermodynamic response in the regime around  $J_{\perp,c}$ , in Fig. 11 we show QMC data for ladders of  $L = 100$  rungs, focusing on the low-temperature region and adding the parameters  $J_{\perp}/J_{\parallel} = 1.5, 1.45, 1.4, 1.35$ , and 1.3 to those already shown in Fig. 9. Clearly the development (and disappearance) of the narrow specific-heat peak is very rapid, being concentrated largely into the region  $1.3 \leq J_{\perp}/J_{\parallel} \leq 1.5$ . The behavior of the specific heat is asymptotically completely symmetrical in the distance

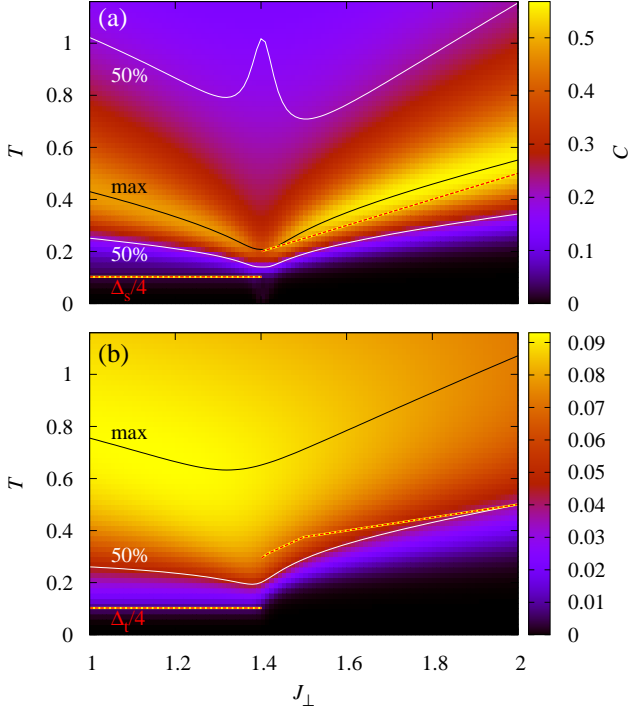


FIG. 10. (Color online) Exact diagonalization results for the specific heat,  $C$  (a), and susceptibility,  $\chi$  (b), of the fully frustrated ladder ( $J_x = J_{\parallel} = 1$ ) with  $L = 14$  rungs, shown for the full range of  $J_{\perp}/J_{\parallel}$  ratios around the transition. Black lines mark the positions,  $T_{\max}^C$  and  $T_{\max}^{\chi}$ , of the peaks in both quantities. White lines mark the temperatures,  $T_{\text{half}}^C$  and  $T_{\text{half}}^{\chi}$ , where they have reached half of the peak height, and for  $C(T)$  the temperature,  $T_u^C$ , where the peak has fallen again to half of the peak height as  $T$  continues to increase. Red-yellow dashed lines mark  $1/4$  of the gaps relevant for each quantity, which for  $C(T)$  is the minimum gap  $\Delta_s$  and for  $\chi(T)$  the triplet gap  $\Delta_t$  (Subsec. II A).

from the transition, as demonstrated by the fact that the results for  $J_{\perp}/J_{\parallel} = 1.38$  and  $1.42$  are difficult to distinguish. The case  $J_{\perp}/J_{\parallel} = 1.4$  lies almost exactly at the transition, where we observe that the low-temperature peak structure is suppressed, leaving only a shoulder feature. Over the same range, the susceptibility exhibits rather little change in its broad maximum,  $\chi_{\max}$ , as a function of the ratio  $J_{\perp}/J_{\parallel}$ , but a quite dramatic drop in the position  $T_{\text{half}}^{\chi}$  of the half-height temperature, which falls by 40% from  $J_{\perp}/J_{\parallel} = 1.5$  to  $1.4$ . As Fig. 10 also makes clear, the evolution of this quantity on the rung-triplet side of the transition is not symmetrical. Again we defer to Sec. V a discussion of how these effects arise in the absence of strong changes to the gap.

We conclude this part of the presentation by returning to Figs. 9(d) and 9(h), which represent a coupling ratio ( $J_{\perp} = J_{\parallel}$ ) deep in the rung-triplet, or Haldane, phase of the ladder. Here we include results for the specific heat and susceptibility of a spin-1 Heisenberg chain [39, 40, 84], which were obtained by QMC simulations

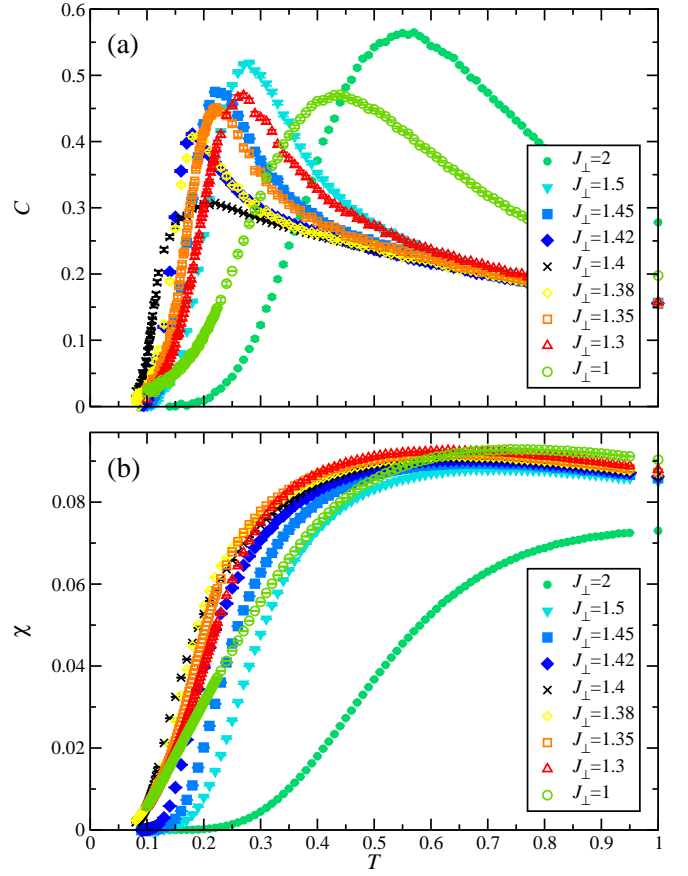


FIG. 11. (Color online) QMC results for the specific heat,  $C$  (a), and susceptibility,  $\chi$  (b), of the fully frustrated ladder ( $J_x = J_{\parallel} = 1$ ) for a range of values of  $J_{\perp}/J_{\parallel}$ .

for chains of 60 sites and are taken from Ref. [43]. Because two  $S = 1/2$  spins on a rung correspond to one spin  $S = 1$ , we have divided by twice the number of spins in the chain for a consistent normalization. The results for the  $J_{\perp} = J_{\parallel}$  ( $= J_x$ ) ladder and the spin-1 chain match completely in their low-temperature asymptotic behavior, reflecting the fact that the low-energy spectra of the two models are identical. However, the maxima of both  $C$  and  $\chi$  appear lower in temperature by a factor of 2 for the ladder than for the spin-1 chain, and the maximum of  $C$  for the ladder is very much higher and sharper. Thus, it is clear that those parts of the ladder Hilbert space with rung spins  $T_i = 0$  remain strongly relevant to the thermodynamic response at all but the lowest temperatures for parameters around  $J_{\perp} = J_{\parallel}$ , and we return to these contributions in Sec. V. As  $J_{\perp}$  is decreased further, states including  $T_i = 0$  rungs are pushed to successively higher energies until the spin-1 Heisenberg chain is recovered from the ladder in the limit  $J_{\perp} \rightarrow -\infty$ .

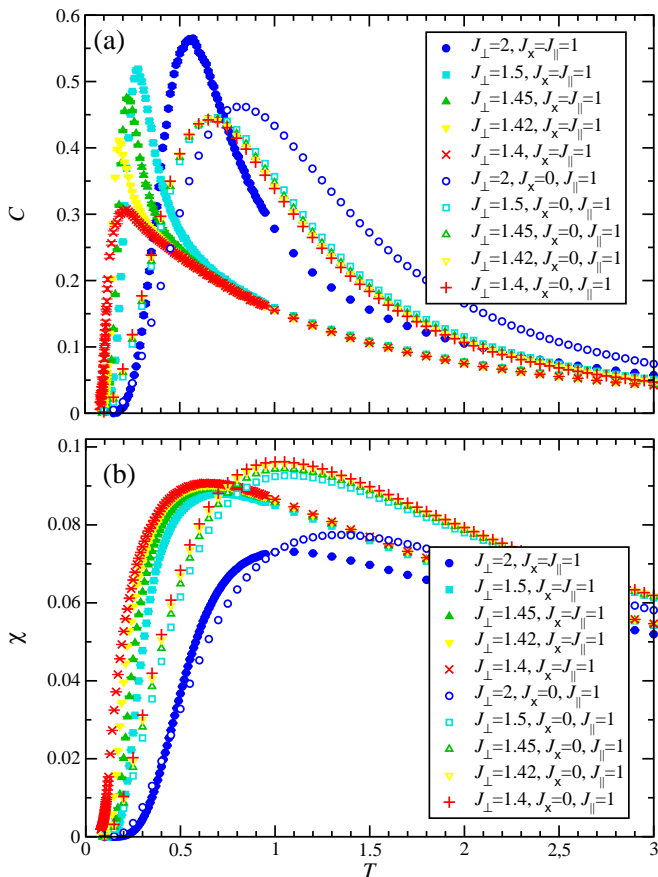


FIG. 12. (Color online) Comparison between the specific heat,  $C$  (a), and susceptibility,  $\chi$  (b), of a fully frustrated ladder ( $J_{\parallel} = J_x = 1$ , closed symbols and crosses) and an unfrustrated ladder ( $J_{\parallel} = 1$ ,  $J_x = 0$ , open and plus symbols) for a range of values of  $J_{\perp}/J_{\parallel}$ . Shown are QMC results for ladders of  $L = 100$  rungs. Error bars on the unfrustrated ladder data are much smaller than the symbol sizes and are omitted.

### C. Frustration Effects

Following Subsec. II B, we use our numerically exact QMC data also to assess the effects of frustration. For this we alter the diagonal (frustrating) coupling,  $J_x$  in Eq. (1), from 1 to 0 in units of  $J_{\parallel}$ , i.e. we consider only the comparison with the unfrustrated ladder but, for reasons of space, avoid a systematic investigation of the crossover between these limits. The unfrustrated  $S = 1/2$  two-leg ladder has been studied in considerable detail [42, 65, 85, 86], including by QMC simulations to obtain the susceptibility [42, 65]. Here we have nevertheless generated our own data for both  $C$  and  $\chi$ , using the SSE QMC technique [75], and the comparison between the two types of ladder is shown in Fig. 12. We restrict our attention again to the coupling region close to the phase transition (the discussion for weaker interdimer coupling may be found in Subsec. II B) and focus only on the rung-singlet regime of the frustrated ladder,  $J_{\perp} \geq 1.4 J_{\parallel}$ , as a comparison is not otherwise meaningful.

The temperature unit in Fig. 12 is the ladder leg coupling,  $J_{\parallel}$ , and thus the results offer a different perspective from that of Subsec. II B, where  $J_{\perp}$  was used. In these units, the specific-heat peak of the unfrustrated ladder moves slowly to lower temperatures as the coupling ratio is reduced. Still, the features of Fig. 5 remain clear at  $J_{\perp} = 2 J_{\parallel}$ , in that the specific heat of the fully frustrated ladder has a significantly narrower and lower-lying maximum than that of the frustrated ladder. As the critical point is approached (3), the peak for the frustrated system shifts rapidly to lower temperatures, falling in height but becoming very much narrower. In the unfrustrated case, by contrast, the specific heat changes very little, as expected for such small variations of the parameters far from a phase transition, and thus stands as a constant benchmark of gap, peak, and broadening effects (Sec. V).

The susceptibilities of the two cases show broadly similar qualitative features, with the positions ( $T_{\max}^{\chi}$ ) of the maxima lying consistently lower in the frustrated than in the unfrustrated system. Dramatic shifts in temperature scales are less apparent in  $T_{\max}^{\chi}$  than in the half-height temperatures,  $T_{\text{half}}^{\chi}$ , with the curves for frustrated ladders moving strongly downward as  $J_{\perp} = 1.4 J_{\parallel}$  is approached, but no comparable behavior for unfrustrated ladders. The heights ( $\chi_{\max}$ ) of the  $\chi$  peaks are quite consistent between the two cases, and notably lower than the decoupled-dimer result (10) shown for comparison with  $J_{\perp} = 2 J_{\parallel}$  in Fig. 9(e), indicating that the effects on  $\chi_{\max}$  of spectral-weight redistribution away from a single energy  $J_{\perp}$  are similar whether this occurs by the opening of a continuous triplon band or of many discrete bound states.

We conclude that the anomalous behavior of both  $C$  and  $\chi$  in the fully frustrated ladder close to  $J_{\perp,c}$  is indeed a signature of the many bound states emerging at low energies close to the frustration-induced first-order transition (Subsec. II A).

## V. INTERPRETATION OF NUMERICAL RESULTS

In this section we compare the numerical results of Sec. IV with different analytical ones to gain further insight into the roles of frustration, of bound states, and of the large numbers of many-triplon bound states at low energies near the phase transition. We first consider the cluster description of Subsec. II B to observe how much of the thermodynamic response is captured by short clusters of different lengths  $n$ . We then consider a large- $n$  description based on the statistical mechanics of unbound domain walls (between singlet and triplet rungs) to capture the unconventional effects of the high density of many-triplon excited states on the specific heat and susceptibility. We conclude by discussing the experimental consequences of and possibilities suggested by our conclusions, emphasizing that, in contrast to conventional gapped quantum magnets,  $C(T)$  and  $\chi(T)$  are

characterized by different gaps and by anomalous effective peak energy scales.

### A. Small-Cluster Analysis

A preliminary interpretation of the numerical results presented in Sec. IV may be obtained by using the cluster approximation of Subsec. IIB to examine the extent to which the exact thermodynamic response functions are reproduced by considering only multi-triplon bound states up to a given size  $n$ . As in Sec. IV, we focus on the region around the phase transition, and of necessity on  $J_{\perp} \geq J_{\perp,c}$  because the cluster approximation is applicable only in the rung-singlet regime. A comparison between the numerically exact results of Fig. 11 and the analytical approximations of Subsec. IIB is presented in Fig. 13 for clusters of 2, 3, and 4 rungs and for five different values of  $J_{\perp}/J_{\parallel}$ . For reference we have also included a curve for the “1-cluster,” which is simply the response of the isolated dimer [Eqs. (9) and (10)].

The cluster approximations for the specific heat [Fig. 13] quantify the results in Figs. 5(b) to 5(d), showing how longer clusters better capture the number of available low-lying states, thereby pushing the peak position,  $T_{\max}^C$ , systematically to lower values. The exact results demonstrate that the simple analytical approach is already accurate at the percent level for  $J_{\perp} = 2J_{\parallel}$  when a cluster of 4 rungs is used [Fig. 13(a)], and by extension it is more accurate still for all values  $J_{\perp} > 2J_{\parallel}$ . This result can be regarded as a consequence of the very short correlation length of the fully frustrated ladder for most values of  $J_{\perp}$  away from the transition region. On closer inspection, the 4-rung approximation actually underestimates  $T_{\max}^C$ , while the 3-rung one overestimates it, illustrating the thermodynamic consequences of the low-lying energy levels shown in Fig. 3 and Table I.

Clearly at  $J_{\perp} = 2J_{\parallel}$  the correction due to longer segments is actually towards energies above the lowest singlet of the 4-rung case. However, as  $J_{\perp}$  is further reduced, the trend of the cluster approximations is primarily to change the peak heights,  $C_{\max}$ , rather than their positions, whereas the peak in the exact data continues to move to lower  $T_{\max}^C$ . This is a clear indication of the importance of the lowest levels in the spectra of ever-longer clusters moving below the one-triplon gap as  $J_{\perp}$  approaches  $J_{\perp,c}$ . At  $J_{\perp} = 1.5J_{\parallel}$  [Fig. 13(b)], the 4-rung cluster is clearly no longer quantitatively adequate, and we comment that not only are extra bound states appearing at lower temperatures (around  $0.3J_{\parallel}$ ) but also at higher ones over a range around  $0.75J_{\parallel}$ . The cluster approximations change rather little in the critical regime [Figs. 13(b) to 13(d)] and the results for  $J_{\perp} = 1.42J_{\parallel}$  [Fig. 13(c)] show clearly the effects of missing the very large numbers of low-lying states illustrated in Figs. 2 and 4, which cause the strong suppression of both  $T_{\max}^C$  and  $C_{\max}$ . We draw attention again to the fact that these changes in the thermodynamic response are not brought

about by changes in the gap, which is captured very well by the smallest cluster ( $n = 2$ , Subsec. IIA); the differences at low temperatures visible below  $J_{\perp} = 1.5J_{\parallel}$  are the consequence of increasing densities of states lying just above the gap.

For the susceptibility, it is clear at  $J_{\perp} = 2J_{\parallel}$  [Fig. 13(f)] that all clusters provide an excellent description of  $\chi(T)$  up to the half-height temperature,  $T_{\text{half}}^{\chi}$ . Above this value, the dominant effect of longer clusters is to reduce the peak height,  $\chi_{\max}$ , and the 3- and 4-rung approximations begin to show a reduction in  $T_{\max}^{\chi}$ . In fact it is the 3-rung approximation that provides the best account of the exact data, with the 4-rung one causing too much suppression, which serves as a reminder that odd- $n$  clusters yield the lowest-lying triplets that govern  $\chi(T)$ . At  $J_{\perp} = 1.5J_{\parallel}$  [Fig. 13(g)], the gaps do begin to differ due to new lowest-lying triplet excitations (Subsec. IIA), and neither the 3- nor the 4-rung approximation provides a good reproduction of the data, presumably reflecting the importance at this coupling ratio of the  $n = 5$  triplet. At  $J_{\perp} = 1.42J_{\parallel}$  [Fig. 13(h)], the peak is by chance rather well described by the  $n = 4$  cluster, but the situation at low  $T$ , where the  $T_{\text{half}}^{\chi}$  temperatures now differ strongly, illustrates the effects of large numbers of magnetic states whose origin lies in multi-triplon clusters with  $n \geq 5$ .

In summary, comparisons between cluster approximations and the exact data show that only small clusters are perfectly sufficient to explain the response of the fully frustrated ladder over much of the rung-singlet regime. However, as the phase transition is approached, large numbers of bound states are moved below the one-triplon excitation energy and their effects are to reduce both the peak energy and the peak height in both  $C$  and  $\chi$ . This demonstration of the importance of many-triplet excitations, and hence of the fact that large clusters ( $n \gg 4$ ) must be considered when calculating thermodynamic properties, even when the system remains gapped, is the fundamental qualitative conclusion of the cluster analysis.

### B. Large-Cluster Analysis

With a view to capturing the rapid changes in thermodynamic response upon approaching  $J_{\perp,c}$ , and the underlying proliferation of low-lying excited states (Fig. 4), we consider a different type of picture based on the predominance of large- $n$  (many-triplon) clusters in the transition regime. This approximation takes clusters to be long and thus the domain walls separating rung singlets ( $T_i = 0$ ) and triplets ( $T_i = 1$ ) to be sparse, such that they may be treated as non-interacting. Although the full spectra of large- $n$  clusters are not known exactly, it is known (Subsec. IIA and Fig. 3) that all many-triplon bound states have a low-lying level whose energy approaches the value  $E_{\text{bond}}$  [Eq. (5)]. A transfer-matrix formulation may be used to sum over the contributions from these levels of

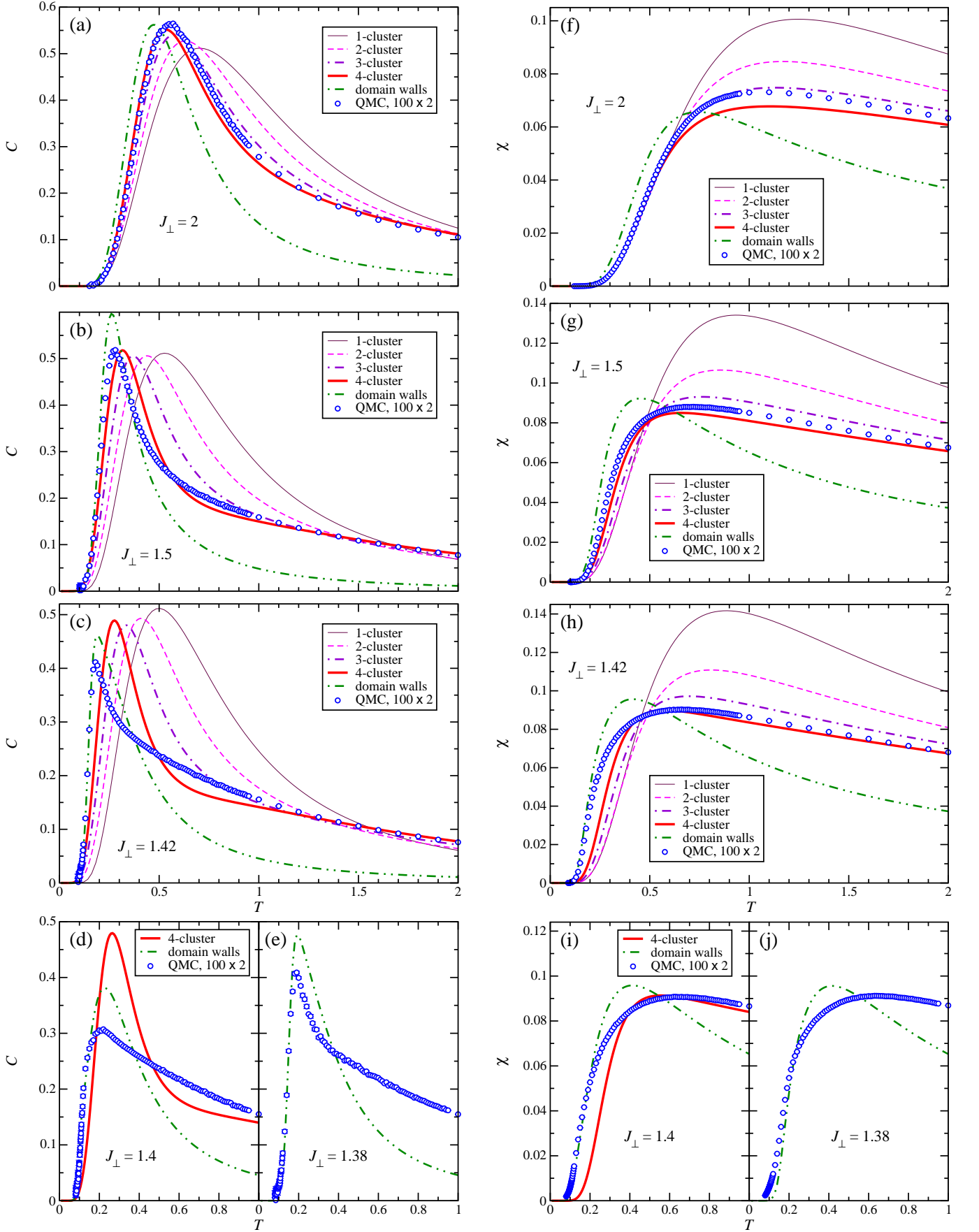


FIG. 13. (Color online) Specific heat,  $C$  (left column), and susceptibility,  $\chi$  (right column), of fully frustrated ladders ( $J_{\times} = J_{\parallel} = 1$ ) with rung coupling ratios  $J_{\perp}/J_{\parallel} = 2, 1.5, 1.42, 1.40,$  and  $1.38$ . QMC results for ladders of  $L = 100$  rungs are compared with approximate calculations based on clusters of 2, 3, and 4 rungs (Subsec. II B) and on non-interacting domain walls (Subsec. V B).

all large- $n$  clusters, providing a suitably size-extensive result expected to be at least qualitatively accurate in a regime where many-triplet bound states dominate the thermodynamic properties.

This treatment is based on the following specific assumptions. i) Each rung in the state  $T_i = 0$  contributes 0 to the total energy. ii) Each rung in the state  $T_i = 1$  contributes  $e_\infty + J_\perp$  to the total energy. iii) Each pair of domain walls contributes an energy  $E_{\text{bond}}$  to the total energy (each domain wall contributes  $E_{\text{bond}}/2$ ). iv) Each domain wall contributes a free spin 1/2, i.e. a two-fold degeneracy. v) There are no interactions between the domain walls. In the parameter regime for which this analysis is designed ( $J_\perp \rightarrow J_{\perp,c}$  from either side), the approximation is clearly not appropriate for small  $n$ , because the neglected binding effects are responsible for the low-energy levels visible on the left side of Fig. 3, but becomes systematically better for larger  $n$ , where many such states accumulate at energies around  $E_{\text{bond}}$ . We comment that this treatment does allow for the occurrence of an odd number of domain walls, although these always appear in pairs on a ladder with periodic boundary conditions, and we expect this to be a legitimate approximation in the region close to the transition, where a finite concentration of domain walls is present.

The gas of non-interacting domain walls can be treated using the standard tools of statistical mechanics [30, 87, 88]. The partition function of the gas of domain walls, whose energetic properties are specified as above, can be computed with the aid of the  $2 \times 2$  transfer matrix

$$\mathcal{T} = \begin{pmatrix} 1 & t(J_\perp, \beta, h) \\ t(J_\perp, \beta, h) & e^{-\beta(e_\infty + J_\perp)} \end{pmatrix}, \quad (12)$$

where the first basis vector of the matrix corresponds to  $T_i = 0$  and the second to  $T_i = 1$ , and

$$t(J_\perp, \beta, h) = 2e^{-\beta(e_\infty + J_\perp + E_{\text{bond}})/2} \cosh(\beta h/2). \quad (13)$$

The arguments of the exponential functions in Eqs. (12) and (13) correspond to the bond energy between rungs  $i$  and  $i+1$  of the ladder, and thus the quantity  $Z_L = \text{Tr} \mathcal{T}^L$  is the sum over the exponentials of the total energies of all such states for a ladder of  $L$  rungs. Because the positions of the domain walls are arbitrary, the state degeneracies are accounted for automatically. The partition function at large  $L$  converges to  $Z_L \approx \lambda_+^L$ , where  $\lambda_+$  is the larger of the two eigenvalues,  $\lambda_\pm$ , of  $\mathcal{T}$ . The expression for  $\lambda_+$  is lengthy and will not be presented here, but we comment that, in the high-temperature limit,  $\lim_{\beta \rightarrow 0} \lambda_+ = 3$ , demonstrating that the domain-wall approximation retains on average three of the four states per rung. By analogy with Eqs. (7) and (8), the specific heat and susceptibility per physical spin are given by

$$C = \frac{\beta^2}{2} \left. \frac{\partial^2}{\partial \beta^2} \ln \lambda_+ \right|_{h=0}, \quad (14)$$

$$\chi = \frac{1}{2\beta} \left. \frac{\partial^2}{\partial h^2} \ln \lambda_+ \right|_{h=0} \quad (15)$$

in the thermodynamic limit ( $L \rightarrow \infty$ ).

By inserting the values of  $e_\infty$  [Eq. (3)] and  $E_{\text{bond}}$  [Eq. (5)], we calculate the specific heat and susceptibility for the values of  $J_\perp/J_\parallel$  shown in Fig. 13. We find that the domain-wall approximation reproduces the evolution of the low-temperature features near  $J_{\perp,c}$  very much better than is possible using the short clusters of Subsec. V A. In both the specific heat [Figs. 13(c) to 13(e)] and the susceptibility [Figs. 13(h) to 13(j)] the exact response given by the QMC data is reproduced with remarkable accuracy up to a temperature of order  $T_{\text{half}}$ . Given that the domain-wall approximation neglects both higher-lying excitations and binding effects, it is not surprising that its accuracy is restricted for high temperatures and far from the transition. However, results for the specific heat in Fig. 13 indicate that the domain-wall description provides an excellent estimate of  $T_{\text{max}}^C$ , although it does overestimate the number of states contributing to  $C_{\text{max}}$ . Because the maximum of the susceptibility appears at higher temperatures, the domain-wall picture is less well suited to describe this feature.

The qualitative and quantitative nature of our results confirms, most importantly, that at the transition a macroscopic number of excitations becomes relevant to the low-temperature thermodynamics of the fully frustrated ladder. Further, these states are well described by non-interacting domain walls between local segments of the ground states on both sides of the transition. We note that  $J_{\perp,c} + e_\infty = 0$  at the transition, and therefore the only remaining energy scale is  $E_{\text{bond}}$ , or more precisely  $E_{\text{bond}}/2 \approx 0.6 J_\parallel$ , which corresponds to the energy cost of a single domain wall. This explains the appearance of the low- $T$  maximum in  $C(T)$  at  $T \approx 0.2 J_\parallel$  when  $J_\perp \approx J_{\perp,c}$ , where a factor of 3 between the intrinsic energy scale and the position of the maximum is typical (cf. Fig. 5). We also comment that, although the domain-wall energy ( $E_{\text{bond}}/2 \approx 0.6 J_\parallel$ ) is larger than the Haldane gap ( $\Delta \approx 0.4 J_\parallel$ ), the domain wall is non-dispersive whereas the magnon of the spin-1 chain has a large bandwidth, and thus domain walls dominate the thermodynamics close to the transition even in the rung-triplet phase [Figs. 13(e) and 13(j)].

### C. Characteristic Energy Scales of $C(T)$ and $\chi(T)$

One may seek to understand the form of the thermodynamic response by extracting the characteristic energy and temperature scales of  $C(T)$  and  $\chi(T)$ . This conventional approach to the response of many low-dimensional models has been discussed in detail in Ref. [42]. It may involve scaling the temperature axis by quantities such as  $T_{\text{max}}$  or the gap,  $\Delta$ , extracted from the low-temperature data, or the  $y$ -axes by the peak heights,  $C_{\text{max}}$  and  $\chi_{\text{max}}$ , to seek similarities and differences between specific aspects of the datasets.

In Fig. 12(a) we compared the specific heats of unfrustrated and frustrated ladders with different coupling

ratios. We found that for unfrustrated ladders, where the (one-triplon) gap,  $\Delta_t$ , falls monotonically with decreasing coupling ratio due to both  $J_\perp$  (band center) and  $J_\parallel$  (band width), the peak position,  $T_{\max}^C$ , decreases only slowly in units of  $J_\parallel$ . By contrast, for frustrated ladders in the rung-singlet regime, the gap ( $\Delta_t = J_\perp$ ) is locked to the coupling ratio for  $J_\perp \geq 2$  and then becomes the singlet gap  $\Delta_s = 2(J_\perp - J_\parallel)$  of the two-triplon bound state as  $J_\perp$  falls towards  $J_{\perp,c}$ , but  $T_{\max}^C$  decreases significantly over this range. This contrast in behavior, in that the gap-to-peak ratio is much larger for frustrated ladders, is clearly visible in Figs. 5(a) to 5(d). If the exponential factor  $e^{-\Delta/T}$  is divided out of the low-temperature data, the remaining prefactor for unfrustrated ladders decreases when scaled to  $J_\perp$ , showing a decreasing density of low-lying states as the relative band width grows. For the frustrated ladders, the increasing prefactor shows the rising density of states close to, but just above, the gap as the quantum phase transition is approached (Subsec. II A).

In the rung-triplet regime, the gap energy scale becomes the Haldane gap, which remains constant as  $J_\perp$  is further reduced and appears quite unconnected to the increase in both  $T_{\max}^C$  and  $C_{\max}$  visible in Fig. 11(a). We have already observed that the Haldane chain does not give a good account of the specific-heat response, except in the very low-temperature limit [Fig. 9(d)]. As at  $J_\perp > J_{\perp,c}$ , the characteristic features of the specific heat for  $J_\perp < J_{\perp,c}$  at intermediate temperatures are dominated by short clusters, this time of rung singlets in a background of rung triplets, which are responsible for the same high density of states near the transition. This conclusion is shown clearly both by the fact (Sec. IV) that the peaks for the rung-singlet and -triplet phases are almost completely symmetrical in their separation from  $J_{\perp,c}$  and by the fact that the domain-wall analysis of Subsec. VB reproduces the high density of states on both sides of  $J_{\perp,c}$ .

Clearly the gap is not a particularly representative scale for the behavior of the specific heat, as may already have been anticipated from the red-yellow dashed lines in Fig. 10(a), which for convenience of presentation show the normalized gap  $\Delta/4$ . Much more representative of the anomalous properties is  $T_{\max}^C$ , shown in the same figure by the black line, which captures the high density of bound states descending to low energies around the transition (Subsec. VB) and thus the corresponding dip in the response temperature. For this reason we do not attempt to scale our numerical data to  $T_{\max}^C$  or  $C_{\max}$ , because the differences between parameter sets are compressed to very small regions at low temperatures.

A further property of the specific heat is the width of its single peak. It is clear in Figs. 9 and 11(a) that the peak becomes very narrow as  $J_\perp \rightarrow J_{\perp,c}$ , but also that its height falls quite abruptly near  $J_{\perp,c}$ , leaving only a shoulder there [Fig. 11(a)]. In Fig. 10(a), we marked with white lines the temperatures,  $T_{\text{half}}^C$  and  $T_u^C$ , where the specific heat has risen to, and then fallen from, its

maximum peak height as  $T$  is increased. Taking their difference as a measure of the peak width, outside the transition region the width does indeed scale with  $T_{\max}^C$ , decreasing as the transition is approached. However, in the region  $1.3 \leq J_\perp \leq 1.5$ ,  $T_u^C$  shows a strong spike, which makes the full-width at half height of the peak rise abruptly. This is a consequence of the rapid drop in peak height, visible in Fig. 11(a) but not reproduced well in either of our analytical approximations. We conclude that the narrowing of the peak is a generic property of the increasing density of low-lying states near the transition due to descending bound-state components, but the vanishing of the peak is a very specific property of the quantum phase transition, where states are distributed quasi-uniformly at many energies above the gap (Fig. 4).

Turning to the susceptibility, in Fig. 12(b) we compared its evolution with coupling ratio for unfrustrated and frustrated ladders. As for the specific heat, in unfrustrated ladders  $T_{\max}^X$  decreases only weakly as the coupling ratio and the gap ( $\Delta_t$ ) both fall. For frustrated ladders in the rung-singlet regime, the relative fall in peak position is much stronger, whereas the triplet gap is precisely  $J_\perp$  over most of the phase diagram, dropping below this only when  $J_\perp \leq 1.5$ , as detailed in Subsec. II A, and therefore has a very limited effect on the properties observed in Fig. 12(b). There is a small increase in  $T_{\max}^X$  as  $J_{\perp,c}$  is approached but, because the maximum of the susceptibility is so broad, a clearer indication of incipient critical behavior can be found from the rapid fall of the half-height temperature,  $T_{\text{half}}^X$ , as  $J_\perp \rightarrow J_{\perp,c}$ . Once again, the low-temperature behavior of all curves in Fig. 12(b) is dictated only by the prefactor of the exponential, which reflects the rising density of triplets close to the gap energy as  $J_\perp \rightarrow J_{\perp,c}$  (Subsec. II A).

In the rung-triplet phase, where the lowest-lying (Haldane) mode is a triplet and the gap is a constant, the peak position of the susceptibility nevertheless moves to higher temperatures as  $J_\perp$  decreases below  $J_{\perp,c}$ . Although in this case the rung-singlet and -triplet sides of the transition are not very symmetrical [Fig. 10(b)], meaning that the relative effect of the Haldane mode is stronger, its contribution still does not account for much of the peak behavior, meaning away from the lowest temperatures [Fig. 9(h)], and this should again be ascribed to short clusters.

Once again, the gap is not a very representative scale for the behavior of the susceptibility of the fully frustrated ladder, as shown by the red-yellow dashed lines in Fig. 10(b) marking 25% of the gap value. In this case, the quantity most representative of the anomalous properties around the transition appears to be  $T_{\text{half}}^X$ , shown in the same figure by the white line. Once again, what is required is to capture the high density of triplet bound states descending to low energies in the vicinity of  $J_{\perp,c}$  (Subsec. VB). In summary, the gaps change rather slowly across the critical region and are in general not the important quantities characterizing either the specific heat or the susceptibility of the fully frustrated ladder away

from the low- $T$  limit. Instead, the falling peak positions are best captured by their temperature scales, which can be related to the low-lying many-triplon bound states of Subsec. II A.

#### D. Experimental Consequences

Despite the importance attached to the gap in low-temperature measurements of thermodynamic quantities in gapped quantum magnets, we have shown here that knowledge of the gap alone does not give much predictive power for the fully frustrated ladder. We draw attention again to the fact that the gaps extracted from the low-temperature behavior of the specific heat and of the susceptibility are not the same; although many frustrated systems are known in theory where low-lying singlet excitations may lie below the triplet gap, this remains very unconventional behavior from the standpoint of experimental observation. We reiterate that the specific heat is a measure of all states in the spectrum and in a frustrated system can be strongly affected by total-spin singlets (usually the lowest-lying states in an antiferromagnet) of multi-particle origin; this is very much the case in the fully frustrated ladder. By contrast, the susceptibility is a measure of finite-spin states only, and is usually dominated by total-spin triplets; multi-particle triplets are also particularly low-lying for odd- $n$  clusters in the fully frustrated ladder and the spin content of all excitations can be understood from the discussion of the spectrum in Subsec. II A.

In the context of the gap, a further valuable experimental quantity to discuss is the correlation length. This is not straightforward to define, but in principle should reflect the zero-range correlations between singlets and triplets on neighboring rungs. Because correlations are developed due to the presence of  $n$ -triplon bound states, the effective correlation length of the system should be an average over the effective cluster length and distribution. Although this average is expected to remain small, close to the phase transition there exist large but transient objects in the form of large- $n$  cluster bound states. We propose that  $1/\Delta$  remains an appropriate measure of the effective correlation length, albeit with two different quantities,  $1/\Delta_s$  and  $1/\Delta_t$ , required to characterize respectively non-magnetic and magnetic correlations near  $J_{\perp,c}$  on the rung-singlet side.

Regarding the direct experimental relevance of our results, we noted in Sec. I that the material  $\text{SrCu}_2(\text{BO}_3)_2$  shows a number of anomalous features in its thermodynamic response. The susceptibility has been found [12] to exhibit a sharp drop at a temperature about one tenth of the dominant coupling energy, whereas the specific heat [13, 14] has a sharp maximum near the same temperature. This system is thought to be a good realization of the (spin-1/2) Shastry-Sutherland model [10, 11], which is intrinsically two-dimensional, but shares two essential features of the fully frustrated ladder. One is that the

one-triplon band is nearly flat, dispersing perhaps due primarily to higher-order Dzyaloshinskii-Moriya interactions. The other is that the magnetic interaction parameters deduced for this compound place it in a dimer-singlet phase, but very close to a quantum phase transition to a different ground state, thought to be a type of plaquette order [89]. Certainly, the trends we observe for the thermodynamic properties of the fully frustrated ladder in the rung-singlet phase close to the transition are remarkably similar to  $\text{SrCu}_2(\text{BO}_3)_2$ , at least for the specific heat. The susceptibility of the ladder model is not as close (Fig. 11), with the temperature scale remaining higher and the maximum appearing more rounded.  $\text{SrCu}_2(\text{BO}_3)_2$  is also known from two-magnon Raman [90, 91] and inelastic neutron scattering measurements [92, 93] to show a highly anomalous thermal evolution of the spectral weight, and this may also be interpreted [94] on the basis of the spectrum in Subsec. II A. We speculate that the type of behavior we have investigated here may arise in other frustrated spin systems with quantum phase transitions.

In this context, it is worth considering the possibilities for the creation of non-thermal transitions in low-dimensional magnets. The most successful approach to date, applied in a number of systems, is the use of a hydrostatic pressure to alter the magnetic exchange interactions and thus to drive the system towards a critical point. In the event that this can be realized, strong changes can be expected in the spectrum that bring many levels to low energies or even to zero. Thus one would have the possibility of observing the type of evolution exhibited here for the fully frustrated ladder not only as a function of temperature but also as a function of pressure at a fixed, low temperature.

Finally, we comment that another prime possibility for the creation of quantum phase transitions is the application of a magnetic field. The field couples only to magnetic states, and the effect would be to bring down one component of all the triplets. In a model as rich as the fully frustrated ladder, with significantly different singlet and triplet spectra, this would cause very strong and inequivalent alterations to  $C$  and  $\chi$ . The phase diagram as a function of applied field and coupling ratio was considered in Ref. [50] in the context of jumps and plateaus in the magnetization curve, whose nature has also been discussed in Ref. [51]. The field-induced transition out of the rung-singlet phase is expected to be first-order, in fact to a mixed rung-singlet/triplet state with no threefold degeneracy on each rung and a finite gap even close to the coupling-induced transition. Because of the dispersive nature of the magnon in the zero-field rung-triplet phase, the field causes a continuous transition and the new ground state is gapless. The fully frustrated ladder in a magnetic field offers a further set of unconventional phenomena related to its exact bound states, flat bands, and high level quasi-degeneracies near the coupling-induced quantum phase transition.

## VI. SUMMARY

We have investigated the thermodynamic properties of the fully frustrated two-leg spin-1/2 ladder. This system exhibits a first-order quantum phase transition between a rung-singlet regime for strong rung coupling and a rung-triplet, or Haldane, phase for weak rung coupling. For all values of the coupling ratio, the system has a gap to all excitations, and the magnetic specific heat and susceptibility are exponentially activated at low temperatures, followed by a single peak. However, in the vicinity of the transition point, the two quantities are characterized by different gaps in the low-energy spectrum on the rung-singlet side, and these gaps, the peaks, peak widths, and peak heights all show a dependence on the coupling constants quite different from reference systems such as the unfrustrated ladder, the spin-1 Heisenberg chain, or the frustrated  $S = 1/2$   $J_1$ - $J_2$  chain.

The physics behind this anomalous behavior lies in the formation of multi-particle bound states. Single-rung excitations are localized objects, and so are their pairs, threesomes, and all higher  $n$ -excitation clusters, which may then be treated as open chains. On approaching the transition point, we observe the formation of large numbers of low-energy states, particularly singlets and triplets of the many-particle clusters, which lead to strongly enhanced fluctuations in this regime. These give rise to a sharp, and anomalously low-temperature, maximum in the specific heat and to an abrupt fall in effective response temperature of the susceptibility, results we show are quite different from the response of unfrustrated ladders. We comment that all of these effects may be expected to have a corresponding signature in the dynamical response function of the fully frustrated ladder at finite temperatures, which is the topic of a companion investigation [94].

We have obtained extremely precise results by detailed numerical calculations using two techniques, ED and QMC, both of which work very well for this model. ED methods are usually restricted to small system sizes, which here we have extended to 28 sites by exploiting the exact relationship between the states of the fully frustrated ladder and of open and closed spin-1 chains. The very short correlation length of the highly frustrated system is also advantageous for capturing most of the physics using a small system. The Hamiltonian in the rung basis (2) also ensures the complete absence of a sign problem in QMC simulations, allowing us to obtain results for ladders up to  $L = 200$  rungs that are demonstrably far into the thermodynamic limit. Elimination of the sign problem by suitable choice of the basis is not new [77], but when applied in models where the total spin of the dimer (or other simplex unit) is conserved gives rise to the possibility of very powerful QMC approaches to frustrated spin systems. The next natural steps in this

context are to test the performance of QMC simulations in the rung basis when the sign problem is not completely eliminated (for example in the ladder model of Eq. (1) with  $J_\times \neq J_\parallel$  [48, 49, 54, 56–59]) and to seek other geometries, interactions, and bases where the sign problem is absent.

Two very general aspects of our results are of direct relevance to experimental studies of low-dimensional frustrated systems. One is the propensity of frustrated systems to bound-state formation, leading to the possibility of high densities of localized (narrow- or flat-band) excitations, which have a strong effect on the physical properties of the system. The other is the effect of proximity to a quantum phase transition, which leads to strong changes in the spectrum and may thus push high densities of states to low energies, with dramatic effects on both the thermodynamic and the dynamical response. Both features may already have been observed in the two-dimensional compound  $\text{SrCu}_2(\text{BO}_3)_2$ , a system whose “Shastry-Sutherland” geometry is so frustrated that the one-triplon band is almost completely flat and whose exchange constants are believed to place it in the dimer-singlet phase (the equivalent of the rung-singlet phase for the ladder), but very near the quantum phase transition to a suspected plaquette state. Indeed the specific heat, susceptibility, and dynamical structure factor measured for this material show some of the anomalous properties we have observed in one dimension in the fully frustrated ladder. The advances of the current work, both in analytical understanding and in numerical capabilities, may be expected to assist in computing the thermodynamic properties of a broad range of frustrated models in the near future.

## ACKNOWLEDGMENTS

We thank H. Rønnow for valuable discussions about  $\text{SrCu}_2(\text{BO}_3)_2$ , H. Tsunetsugu, and W.-Q. Yu for helpful comments, and N. Chepiga for sharing with us some unpublished DMRG data for  $S = 1$  chains. We are particularly grateful to F. Alet and K. Damle for discussions concerning the spin-dimer basis for QMC and for pointing out the feasibility of avoiding the QMC sign problem with additional  $D^z D^z$  terms only. Methodological ideas and QMC results similar to ours for the fully frustrated ladder are reported in Ref. [82]. We acknowledge the ALPS numerical libraries [95, 96], with which preliminary QMC simulations were performed. This work was supported by the DFG under Grant FOR1807, by the NSF of China under Grant 11174365, and by the National Basic Research Program of the Chinese MoST under Grant 2012CB921704. SW acknowledges the hospitality of ECT\* (Trento) and the allocation of CPU time at JSC Jülich and RWTH Aachen through JARA-HPC. FM thanks the Paul Scherrer Institute for hospitality and the Swiss National Science Foundation for support.

- 
- [1] W. Heisenberg, *Z. Phys.* **49**, 619 (1928).
- [2] H.-J. Mikeska and A. K. Kolezhuk, *Lect. Notes Phys.* **645**, 1 (2004).
- [3] F. D. M. Haldane, *Phys. Rev. Lett.* **50**, 1153 (1983); *Phys. Lett. A* **93**, 464 (1983).
- [4] C. K. Majumdar and D. Ghosh, *J. Math. Phys.* **10**, 1388 (1969).
- [5] C. K. Majumdar, *J. Phys. C: Solid State Phys.* **3**, 911 (1969).
- [6] J. Richter, J. Schulenburg, and A. Honecker, *Lect. Notes Phys.* **645**, 85 (2004).
- [7] L. Balents, *Nature* **464**, 199 (2010).
- [8] *Introduction to Frustrated Magnetism: Materials, Experiments, Theory*, edited by C. Lacroix, P. Mendels, and F. Mila, Springer Series in Solid-State Sciences (Springer, Berlin, 2011).
- [9] *Frustrated Spin Systems*, 2<sup>nd</sup> edition, edited by H. T. Diep (World Scientific, Singapore, 2013).
- [10] B. S. Shastry and B. Sutherland, *Physica B & C* **108**, 1069 (1981).
- [11] S. Miyahara and K. Ueda, *J. Phys.: Condens. Matter* **15**, R327 (2003).
- [12] H. Kageyama, K. Yoshimura, R. Stern, N. V. Mushnikov, K. Onizuka, M. Kato, K. Kosuge, C. P. Slichter, T. Goto, and Y. Ueda, *Phys. Rev. Lett.* **82**, 3168 (1999).
- [13] H. Kageyama, K. Onizuka, Y. Ueda, M. Nohara, H. Suzuki, and H. Takagi, *J. Exp. Theor. Phys.* **90**, 129 (2000).
- [14] H. Kageyama, H. Suzuki, M. Nohara, K. Onizuka, H. Takagi, and Y. Ueda, *Physica B* **281-282**, 667 (2000).
- [15] H. Kageyama, K. Onizuka, T. Yamauchi, Y. Ueda, S. Hane, H. Mitamura, T. Goto, K. Yoshimura, and K. Kosuge, *J. Phys. Soc. Jpn.* **68**, 1821 (1999).
- [16] K. Kodama, M. Takigawa, M. Horvatić, C. Berthier, H. Kageyama, Y. Ueda, S. Miyahara, F. Becca, and F. Mila, *Science* **298**, 395 (2002).
- [17] M. Jaime, R. Daou, S. A. Crooker, F. Weickert, A. Uchida, A. E. Feiguin, C. D. Batista, H. A. Dabkowska, and B. D. Gaulin, *Proc. Natl. Acad. Sci. U.S.A.* **109**, 12404 (2012).
- [18] Y. H. Matsuda, N. Abe, S. Takeyama, H. Kageyama, P. Corboz, A. Honecker, S. R. Manmana, G. R. Foltin, K. P. Schmidt, and F. Mila, *Phys. Rev. Lett.* **111**, 137204 (2013).
- [19] T. Momoi and K. Totsuka, *Phys. Rev. B* **62**, 15067 (2000).
- [20] Weihong Zheng, C. J. Hamer, R. R. P. Singh, S. Trebst, and H. Monien, *Phys. Rev. B* **63**, 144410 (2001).
- [21] M. Windt, M. Grüninger, T. Nunner, C. Knetter, K. P. Schmidt, G. S. Uhrig, T. Kopp, A. Freimuth, U. Ammerahl, B. Büchner, and A. Revcolevschi, *Phys. Rev. Lett.* **87**, 127002 (2001).
- [22] C. Knetter, A. Bühler, E. Müller-Hartmann, and G. S. Uhrig, *Phys. Rev. Lett.* **85**, 3958 (2000).
- [23] M. Takahashi, *Thermodynamics of One-dimensional Solvable Models* (Cambridge University Press, Cambridge, 1999).
- [24] M. Gaudin, *Phys. Rev. Lett.* **26**, 1301 (1971).
- [25] S. Eggert, I. Affleck, and M. Takahashi, *Phys. Rev. Lett.* **73**, 332 (1994).
- [26] A. Klümper, *Eur. Phys. J. B* **5**, 677 (1998).
- [27] A. Klümper and D. C. Johnston, *Phys. Rev. Lett.* **84**, 4701 (2000).
- [28] C. Trippé, A. Honecker, A. Klümper, and V. Ohanyan, *Phys. Rev. B* **81**, 054402 (2010).
- [29] H. Bethe, *Z. Phys.* **71**, 205 (1931).
- [30] R. Baxter, *Exactly Solved Models in Statistical Mechanics* (Academic, New York, 1982).
- [31] J. C. Bonner and M. E. Fisher, *Phys. Rev.* **135**, A640 (1964).
- [32] F. Heidrich-Meisner, A. Honecker, and T. Vekua, *Phys. Rev. B* **74**, 020403(R) (2006).
- [33] *Phase Transitions and Critical Phenomena: Series expansion for lattice models*, Vol. 3, edited by C. Domb and M. S. Green (Academic Press, London, 1974).
- [34] H.-J. Schmidt, A. Lohmann, and J. Richter, *Phys. Rev. B* **84**, 104443 (2011).
- [35] A. Lohmann, H.-J. Schmidt, and J. Richter, *Phys. Rev. B* **89**, 014415 (2014).
- [36] Zheng Weihong, C. J. Hamer, and J. Oitmaa, *Phys. Rev. B* **60**, 6608 (1999).
- [37] S. R. White, *Phys. Rev. Lett.* **69**, 2863 (1992); *Phys. Rev. B* **48**, 10345 (1993).
- [38] X. Wang and T. Xiang, *Phys. Rev. B* **56**, 5061 (1997).
- [39] T. Xiang, *Phys. Rev. B* **58**, 9142 (1998).
- [40] A. E. Feiguin and S. R. White, *Phys. Rev. B* **72**, 220401(R) (2005).
- [41] U. Schollwöck, *Ann. Phys.* **326**, 96 (2011).
- [42] D. C. Johnston, M. Troyer, S. Miyahara, D. Lidsky, K. Ueda, M. Azuma, Z. Hiroi, M. Takano, M. Isobe, Y. Ueda, M. A. Korotin, V. I. Anisimov, A. V. Mahajan, and L. L. Miller, unpublished ([arXiv:cond-mat/0001147v1](https://arxiv.org/abs/cond-mat/0001147v1)).
- [43] A. Niazi, S. L. Bud'ko, D. L. Schlagel, J. Q. Yan, T. A. Lograsso, A. Kreyssig, S. Das, S. Nandi, A. I. Goldman, A. Honecker, R. W. McCallum, M. Reehuis, O. Pieper, B. Lake, and D. C. Johnston, *Phys. Rev. B* **79**, 104432 (2009).
- [44] D. C. Johnston, R. J. McQueeney, B. Lake, A. Honecker, M. E. Zhitomirsky, R. Nath, Y. Furukawa, V. P. Antropov, and Y. Singh, *Phys. Rev. B* **84**, 094445 (2011).
- [45] M. P. Gelfand, *Phys. Rev. B* **43**, 8644 (1991).
- [46] I. Bose and S. Gayen, *Phys. Rev. B* **48**, 10653(R) (1993).
- [47] Y. Xian, *Phys. Rev. B* **52**, 12485 (1995).
- [48] Zheng Weihong, V. Kotov, and J. Oitmaa, *Phys. Rev. B* **57**, 11439 (1998).
- [49] X. Wang, *Mod. Phys. Lett. B* **14**, 327 (2000).
- [50] A. Honecker, F. Mila, and M. Troyer, *Eur. Phys. J. B* **15**, 227 (2000).
- [51] C. A. Lamas and J. M. Matera, *Phys. Rev. B* **92**, 115111 (2015).
- [52] W. Brenig and K. W. Becker, *Phys. Rev. B* **64**, 214413 (2001).
- [53] K. Totsuka and H.-J. Mikeska, *Phys. Rev. B* **66**, 054435 (2002).
- [54] O. A. Starykh and L. Balents, *Phys. Rev. Lett.* **93**, 127202 (2004).
- [55] T. Vekua and A. Honecker, *Phys. Rev. B* **73**, 214427 (2006).
- [56] E. H. Kim, Ö. Legeza, and J. Sólyom, *Phys. Rev. B* **77**, 205121 (2008).
- [57] T. Hikihara and O. A. Starykh, *Phys. Rev. B* **81**, 064432 (2010).

- [58] D. Poilblanc, *Phys. Rev. Lett.* **105**, 077202 (2010).
- [59] X.-H. Chen, S. Y. Cho, M. T. Batchelor, H.-Q. Zhou, unpublished ([arXiv:1508.03941v1](https://arxiv.org/abs/1508.03941v1)).
- [60] S. R. White and D. A. Huse, *Phys. Rev. B* **48**, 3844 (1993).
- [61] O. Golinelli, T. Jolicoeur, and R. Lacaze, *Phys. Rev. B* **50**, 3037 (1994).
- [62] T. Kennedy, *J. Phys.: Condens. Matter* **2**, 5737 (1990).
- [63] I. Affleck, T. Kennedy, E. H. Lieb, and H. Tasaki, *Phys. Rev. Lett.* **59**, 799 (1987).
- [64] B. Normand and Ch. Rüegg, *Phys. Rev. B* **83**, 054415 (2011).
- [65] B. Frischmuth, B. Ammon, and M. Troyer, *Phys. Rev. B* **54**, R3714 (1996).
- [66] M. Greven, R. J. Birgeneau, and U. J. Wiese, *Phys. Rev. Lett.* **77**, 1865 (1996).
- [67] B. Bleaney and K. D. Bowers, *Proc. R. Soc. London, Ser. A* **214**, 451 (1952).
- [68] D. C. Johnston, R. K. Kremer, M. Troyer, X. Wang, A. Klümper, S. L. Bud'ko, A. F. Panchula, and P. C. Canfield, *Phys. Rev. B* **61**, 9558 (2000).
- [69] J. Deisenhofer, R. M. Eremina, A. Pimenov, T. Gavrilova, H. Berger, M. Johnsson, P. Lemmens, H.-A. Krug von Nidda, A. Loidl, K.-S. Lee, and M.-H. Whangbo, *Phys. Rev. B* **74**, 174421 (2006).
- [70] O. Derzhko, J. Richter, A. Honecker, and H.-J. Schmidt, *Low Temp. Phys.* **33**, 745 (2007).
- [71] A. Honecker, S. Hu, R. Peters, and J. Richter, *J. Phys.: Condens. Matter* **23**, 164211 (2011).
- [72] V. Ohanyan and A. Honecker, *Phys. Rev. B* **86**, 054412 (2012).
- [73] C. Lanczos, *J. Res. Nat. Bur. Stand.* **45**, 255 (1950).
- [74] E. Dagotto, *Rev. Mod. Phys.* **66**, 763 (1994).
- [75] O. F. Syljuåsen and A. W. Sandvik, *Phys. Rev. E* **66**, 046701 (2002).
- [76] M. Troyer and U.-J. Wiese, *Phys. Rev. Lett.* **94**, 170201 (2005).
- [77] T. Nakamura, *Phys. Rev. B* **57**, R3197 (1998).
- [78] F. Alet, S. Wessel, and M. Troyer, *Phys. Rev. E* **71**, 036706 (2005).
- [79] K. Hukushima, H. Takayama, and K. Nemoto, *Int. J. Mod. Phys. C* **7**, 337 (1996).
- [80] K. Hukushima and K. Nemoto, *J. Phys. Soc. Jpn.* **65**, 1604 (1996).
- [81] E. Marinari, *Lect. Notes in Phys.* **501**, 50 (1998).
- [82] F. Alet, K. Damle, and S. Pujari, unpublished.
- [83] M. Mambri, J. Trébos, and F. Mila, *Phys. Rev. B* **59**, 13806 (1999).
- [84] S. Yamamoto and S. Miyashita, *Phys. Rev. B* **48**, 9528 (1993).
- [85] Zheng Weihong, R. R. P. Singh, and J. Oitmaa, *Phys. Rev. B* **55**, 8052 (1997).
- [86] Q. Gu, D.-K. Yu, and J.-L. Shen, *Phys. Rev. B* **60**, 3009 (1999).
- [87] E. Ising, *Z. Phys.* **31**, 253 (1925).
- [88] K. Huang, *Statistical Mechanics* (Wiley, New York, 1963).
- [89] P. Corboz and F. Mila, *Phys. Rev. B* **87**, 115144 (2013).
- [90] P. Lemmens, M. Grove, M. Fischer, G. Güntherodt, V. N. Kotov, H. Kageyama, K. Onizuka, and Y. Ueda, *Phys. Rev. Lett.* **85**, 2605 (2000).
- [91] A. Gozar, B. S. Dennis, H. Kageyama, and G. Blumberg, *Phys. Rev. B* **72**, 064405 (2005).
- [92] B. D. Gaulin, S. H. Lee, S. Haravifard, J. P. Castellán, A. J. Berlinsky, H. A. Dabkowska, Y. Qiu, and J. R. D. Copley, *Phys. Rev. Lett.* **93**, 267202 (2004).
- [93] M. E. Zayed, Ch. Rüegg, Th. Strässle, U. Stühr, B. Roessli, M. Ay, J. Mesot, P. Link, E. Pomjakushina, M. Stingaciu, K. Conder, and H. M. Rønnow, *Phys. Rev. Lett.* **113**, 067201 (2014).
- [94] A. Honecker, F. Mila, and B. Normand, unpublished.
- [95] M. Troyer, B. Ammon, and E. Heeb, *Lect. Notes Comp. Sci.* **1505**, 191 (1998).
- [96] A. F. Albuquerque, F. Alet, P. Corboz, P. Dayal, A. Feiguin, S. Fuchs, L. Gamper, E. Gull, S. Gürtler, A. Honecker, R. Igarashi, M. Körner, A. Kozhevnikov, A. Läuchli, S. R. Manmana, M. Matsumoto, I. P. McCulloch, F. Michel, R. M. Noack, G. Pawłowski, L. Pollet, T. Pruschke, U. Schollwöck, S. Todo, S. Trebst, M. Troyer, P. Werner, and S. Wessel, *J. Magn. Magn. Mater.* **310**, 1187 (2007).